DEVELOPMENT OF A NECK PALPATION DEVICE FOR TELEMEDICAL ENVIRONMENTS

By

David Jacobus van den Heever

Thesis presented at the University of Stellenbosch
in partial fulfillment of the requirements of the
degree of

Master of Science in Mechatronic Engineering

Department of Mechanical and Mechatronic Engineering
University of Stellenbosch
Private Bag X1, 7602, Matieland, South Africa

Supervisors
Dr. K. Schreve
Prof. C. Scheffer

November 2007

DECLARATION

I, the undersigned, hereby declare that the work contained in this thesis is my own original work and that I have not previously in its entirety or in part submitted it at any university for a degree.

Signature: ---------- Date: ----------

SUMMARY

An abnormal sized mass in the neck is a common clinical finding and it can be the result of inflammation caused by bacterial or viral infection or it can be due to more serious diseases and malignant tumours. The most popular method of examining the neck is by manual palpation. Other methods include ultrasound, CT scan, MRI and PET. These methods though are expensive to perform and require specialists to interpret the results. The aim of this thesis was to design and develop a neck palpation device for telemedicine applications.

The device uses an array of Force Sensing Resistors (FSRs) attached to an inflatable bladder. The bladder is mounted to the inside of a neck brace and it is inflated with an air pump controlled by a computer. As the bladder inflates the sensors press against the patient's neck and the necessary data can be collected. A technique known as image registration is used to improve the resolution of the images sensed with the FSRs.

The device provides a reproducible record of the examination for both the surgeon and the patient's medical record, and provides the patient information as if the doctor examined the patient with his own hands without physically being there. A prototype of the device was built and used to perform numerous tests. The tests were conducted using different objects which are inserted into a silicone neck to simulate different lymph nodes. The device was used to test for shape, smallest size, different sizes, repeatability and hardness.

The results showed that the device works well for spherical objects of different sizes but gives unsatisfactory results when the objects have sharp edges and complex forms. The image registration algorithm enhanced the images to a good representation of the object. Different sizes could be distinguished as well as hardness to some extend.

OPSOMMING

‘n Abnormaal groot massa in die nek is ‘n algemene kliniese vinding en dit kan die resultaat wees van inflamasie deur bakterie of virale infeksie, of dit kan veroorsaak wees deur meer ernstige siektes en gewasse. Die mees populêre metode om die nek te ondersek is om die nek met die hande te betas. Ander metodes sluit in ultraklank, CT skandeering, MRI en PET. Hierdie metodes is egter duur om uit te voer en dit benodig spesialiste om die resultate te interpreteer. The hoof doel van die tesis was om ’n nek tas toestel te ontwikkel vir telemedisyne omgewings.

Die toestel gebruik ’n matriks van krag sensitiewe weerstande (FSRs) wat vas is aan ’n opblaasbare rubber stuk. Hierdie rubber stuk is gemonteer aan die binne kant van ’n nek stut en dit word opgeblaas deur ’n lug pomp wat beheer word deur ’n rekenaar. Soos die rubber stuk opblaas, druk die sensors teen die pasiënt se nek en die nodige data word geneem. ’n Tegniek bekend as beeld registrasie word gebruik om die resolusie van die beelde geneem met die FSRs te verbeter.

Die toestel lewer ’n herhaalbare rekord van die ondersoek vir beide die dokter en die pasiënt se mediese rekord. Verder lewer die toestel ook die informasie asof die pasiënt deur ’n dokter se hande ondersoek was, sonder dat die dokter ooit werklik teenwoordig was. ’n Prototipe van die toestel is gebou en gebruik om talle toetse te doen. Die toetse is uitgevoer met die gebruik van verskillende voorwerpe wat in ’n silikon nek geplaas is om die limf nodes voor te stel. Die toestel was gebruik om te toets vir vorm, kleinste voorwerp, verskillende groottes, herhaalbaarheid en hardheid.

Die resultate wys dat die toestel goed werk vir sferiese voorwerpe van verskillende groottes, maar die toestel lewer ongewensde resultate wanneer die voorwerpe skerp hoeke het en komplekse vorms aanneem. Die beeld registrasie algoritme het die resolusie van die beelde genoegsaam verbeter. Verskillende groottes kon onderskei word asook hardheid tot ’n mate.

ACKNOWLEDGEMENTS

The following people are thanked for their valuable input in making this thesis a success:

Dr. Kristiaan Schreve
Prof. Cornie Scheffer
Stefan van der Walt
Sven Queisser
Alexander Bögel
Dirk Koekemoer
Alfred Coupe

TABLE OF CONTENTS

LIST OF FIGURES

LIST OF TABLES

LIST OF ACRONYMS

A/D	Analog/Digital
ABS	Anti-lock Braking System
BJT	Bipolar Junction Transistor
CT	Computed Tomography
FSR	Force Sensing Resistor
LMA	Levenberg Marquardt Algorithm
MRI	Magnetic Resonance Imaging
MTI	Medical Tactile Inc
NiCr	Nickel Chrome
NMR	Nuclear Magnetic Resonance
PET	Positron Emission Tomography
PIC	Programmable Integrated Circuit
PID	Proportional Integral Differential
PLC	Programmable Logic Control
PVDF	Polyvinylidene Fluoride
QFD	Quality Function Deployment
RTD	Resistance Temperature Device
UART	Universal Asynchronous Receiver/ Transmitter
VLSI	Very Large Scale Integration

1. INTRODUCTION

During a routine clinical examination of a patient, the health care provider will investigate the main organ systems by inspection, palpation, percussion and auscultation. A common finding during this investigation is an abnormal-sized mass in the neck [1]. The cause can be the result of inflammation caused by bacterial or viral infection or it can be due to more serious diseases or malignant tumours. Manual palpation of the neck area is the oldest and most established method of all neck examinations. Unfortunately, clinical palpation of the neck demonstrates a large variation of findings among various examiners, according to Gosselin [1]. Although palpation is inexpensive, findings are generally accepted as inaccurate. Gosselin states a typical range of 60-70% for sensitivity and specificity, depending on the size and type of tumour in the neck.

Other methods that are used to examine the neck include ultrasound, computed tomography (CT), magnetic resonance imaging (MRI) and positron emission topography (PET). However, all of these methods require a specially trained person to operate the devices and interpret the results. The apparatus and facilities used are also expensive to use and maintain which makes these methods more expensive than manual palpation by a health care provider.

The goal of this project is to design and manufacture a prototype of a neck palpation device for telemedicine applications. Telemedicine refers to the use of communications and information technology for delivering clinical or medical care. Telemedicine can therefore play a major role in rural healthcare in underserved areas by providing specialists with the necessary information. These specialists can be located anywhere in the world and still provide advice or a diagnosis.

The proposed device should be a semi-automated electro-mechanical device capable of collecting the same information as manual palpation. The data collected by the device must be presented in a user-friendly format that can be sent to a medical doctor to make a diagnosis. It is envisaged that the device can be automated in such a way that it can be operated by a trained nurse for use in conjunction with other telemedical devices in rural areas where doctors are scarce. The device provides a reproducible record of the examination for both the doctor and the patient's medical record, and provides the patient information as if the doctor examined the patient with his own hands without physically being there. The prototype device will be tested using a silicone neck and different-sized objects to simulate different lymph

nodes. Clinical testing of the device was not performed for this study and it is considered as future work.

No mention of neck palpation devices were found in the literature although there are palpation devices available which are normally used for breast examination such as SureTouch Visual Mapping System [2]. These devices normally consist of a handheld transducer with hundreds of tiny pressure sensors on the footplate of the transducer. These sensors each measure the relative firmness of the breast underneath the transducer.

The report will follow the following order. Chapter 2 will look at the motivation and goals of the project. The literature study is discussed in Chapter 3. The literature study gives a short background description followed by literature on tactile sensing as well as image registration. Chapter 4 looks at the different concepts and ideas that was investigated and their respective advantages and disadvantages. This is followed by a discussion on the design of the final prototype in Chapter 5. An artificial neck made to perform the tests on will be discussed in Chapter 6, followed by the testing and results in Chapters 7 and 8. In conclusion the report will look at the contribution of the thesis project and further work that can be done.

2. MOTIVATION AND GOALS

According to the world health report of 2000 [3], more than half the African countries have a life expectancy below 40 years. This is due to the lack of proper health care structures in these countries. Telemedicine methods or systems can be used to improve the health care in these countries and ultimately improve the life expectancy.

With telemedicine, a medical specialist in a first world country can consult with a health care provider (not necessarily a doctor) in an underserved African country. The medical specialist's expertise can save a patient's life without him ever having to see or communicate with the patient. All that is required is the necessary information regarding the patient's history and symptoms.

Thus the goal of this project is to develop a neck palpation device which fulfills the following requirements:

- A nurse with some basic training must be able to operate the device.
- Must gather the required information, mimicking the information gathered during manual palpation.
- Produce a reproducible, easy to understand record of the examination.
- Produce this record in an electronic format.
- Device must be cost-effective.

3. LITERATURE STUDY

An overview of relevant literature is presented here. It is divided into the following three sections:

1. Background
2. Tactile sensing
3. Image registration

The first section will look at the required background needed for the project which includes the physiology of the lymphatic system and the specific parameters a physician will investigate during a clinical examination. Other recognized methods of detecting will be investigated. The second section deals with tactile sensing and describes numerous tactile sensing techniques. This is an important field to investigate when looking to recreate the sense of touch. The last section discusses image registration, a set of techniques and methods that was used to improve the quality of the measured images.

BACKGROUND

Lymph nodes form part of the lymphatic system. It produces and distributes lymphocytes which are vital to our ability to resist or overcome infection and disease. Lymphocytes respond to the presence of:

- invading pathogens such as bacteria or viruses,
- abnormal body cells, such as virus-infected cells or cancer cells, and
- foreign proteins, such as the toxins released by some bacteria [4]

A fluid called lymph flows through the lymphatic vessels and lymph nodes. The lymph nodes act as a filter and purify the lymph before it reaches the venous system. As lymph flows through a lymph node, at least 99% of the antigens present in the arriving lymph will be removed and this stimulates lymphocytes which triggers an immune response. Lymph nodes are located in regions where they can detect and eliminate harmful “intruders” before they reach vital organs of the body. Figure 1 shows the positions of the lymph nodes in the neck area.

Chronic or excessive enlargement of lymph nodes may occur in response to bacterial or viral infections, endocrine disorders, or cancer. Since the lymphatic capillaries offer little resistance to the passage of cancer cells, cancer cells often spread along the lymphatics and become

trapped in the lymph nodes. Thus, the analysis of swollen lymph nodes can provide information on the distribution and nature of the cancer cells, aiding in the selection of appropriate therapies. Lymphomas are an important group of lymphatic system cancers.

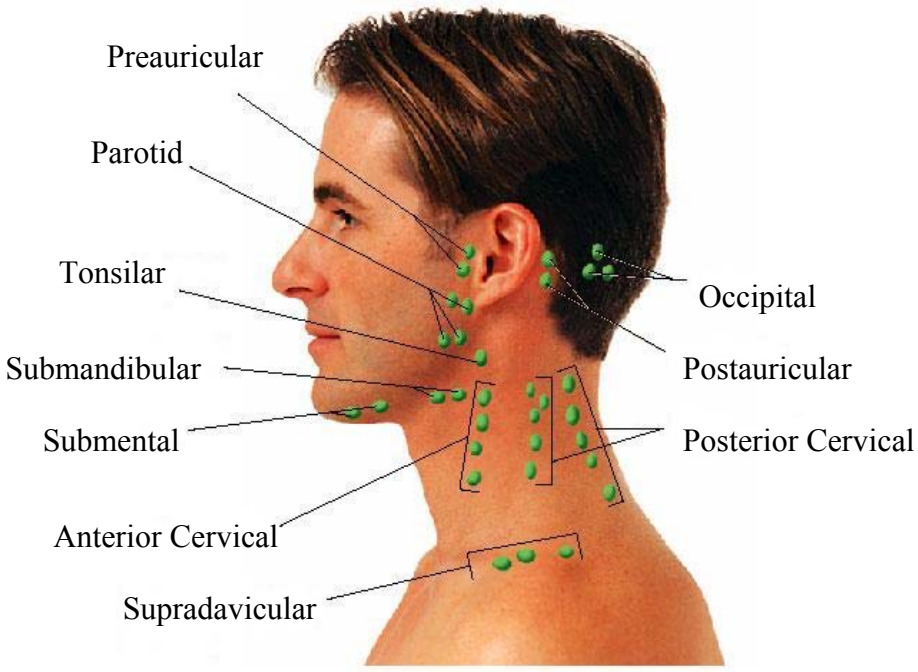

Figure 1: Lymph nodes in the neck area [5]

During a clinical examination of the neck, the physician will pay specific attention to the location, size, firmness and mobility of each node. Unhealthy lymph nodes generally increase in size over time and are usually greater than 15 mm in size. Unhealthy lymph nodes are also firm, non-tender, matted, the mobility is decreased or it's completely fixed and the temperature in the area of the node is increased. These are the usual signs a doctor will look for when performing the diagnosis.

A description of each node is an important part of the medical record, which can be used to assess the response to the treatment or the progression of the disease. Typical record entrees consist of a short description of the findings accompanied by simple hand drawn figures. These drawings however are subjective and rely heavily on the opinion of the physician. There is no standard or formal structure for these drawings and thus attempts to use these drawings by other physicians have proven difficult according to Kaufman [6].

Other means of detecting unhealthy nodes like ultrasound, computed tomography (CT scan), magnetic resonance imaging (MRI) and positron emission tomography (PET) address this problem by providing an image of the examined area. These images however are difficult to interpret and require a specialist to examine them. Table 1 compares these different methods against a few important factors. Appendix A gives a more detailed description of each method.

Table 1: Comparison of Imaging Modalities

	Ultrasound	**CT**	**MRI**	**PET**
Description [7],[8],[9],[10]	High-energy sound waves bounce off internal tissues and produce echoes. These echo patterns are shown on a screen.	A large number of 2D x-ray images are taken at discrete sections. A 3D image is then produced by employing tomography (imaging by sections).	Uses non-ionizing radio frequency signals to acquire images. MRI relies on the relaxation properties (spin) of excited hydrogen nuclei in a magnetic field.	Uses a short-lived radioactive tracer isotope which is injected into subject. The isotope decays and emits a positron which is detected.
What is imaged [7]	Mechanical properties	Tissue absorption	Biochemistry	Photons
Required access [7]	Small windows adequate	Circumferential around body	Circumferential around body	Circumferential around body
Spatial resolution[7], [9]	0.3 to 3 mm	~ 1 mm	~ 1 mm	~ 1 mm
Safety [7]	Fair	Ionizing radiation	Good	Ionizing radiation
Speed [7]	100 frames per second	Half-minute to minutes	Minutes	Waiting period for isotope is 1 hour
Cost [7], [8]	$	$$$	$$$$$$	$$$$
Portability [7]	Excellent	Poor	Poor	Poor

Although all of the methods in Table 1 produce better images of the examined area, and may well give more accurate results than a clinical examination performed by a physician, these methods have their disadvantages. Ultrasound enhances inflammatory response, it can heat

soft tissue and the borders on the images are poorly defined which makes interpretation difficult [10]. On the other hand, CT scan and PET have radiation effects. All of these methods, except for ultrasound, use expensive and complex apparatus which makes a quick check-up impossible.

All of these limitations and the progress made in tactile sensing over the last few years, has been the driving force in developing new methods for examination.

TACTILE SENSING

Tactile sensing is the measurement of the parameters of a contact between a sensor and an object. Crowder [11] defines tactile sensing as "…the detection and measurement of the spatial distribution of forces perpendicular to a predetermined sensory area, and the subsequent interpretation of the spatial information". Tactile sensors can be used to measure a wide variety of stimuli particularly in different biomedical applications. In order to improve the efficiency of these sensors, a tactile-sensing array can be utilized [12-14]. A tactile-sensing array can be considered to be a coordinated group of touch sensors.

The following two sections will look at tactile sensing in industrial and medical applications.

3.2.1 Tactile sensing for industrial applications

Crowder [11] investigated tactile sensing specifically for industrial applications and defined the following as desirable characteristics for a touch or tactile sensor:

- A single touch sensor should ideally be as small as possible. Taking the difficulty of fabricating miniature sensing elements into consideration, a sensing area of 1-2 mm^2 is proposed.
- A sensitivity range of 0.4 – 10 N, together with an allowance for accidental mechanical overload.
- Frequency range of 0 - 100 Hz.
- Stable and repeatable characteristics.
- Low hysteresis.
- Sensor must be robust and protected from environmental damage.

- For a tactile array, an array of 10 – 20 sensors square is proposed.

With these specifications in mind, different tactile sensors used for industrial applications have been developed. A more detailed description of these different sensors can be found in Appendix B.

Crowder [11] describes the **mechanically-based sensor** as the simplest form of touch sensor. An applied force is used to activate a conventional mechanical switch to form a binary touch sensor. This gives no indication of the magnitude of the applied force though. A **resistive based sensor** uses a material with a defined force-resistance characteristic. The measurement of the resistance between two points on this material, usually a conductive elastomer or foam, gives an indication of the applied force.

A **capacitive-based sensor** relies on the applied force changing the distance between two parallel plates or the effective surface area of the capacitor [15]. This will change the capacitance of the system which can be detected. Matsuzaki and Todoroki [16] propose a flexible patch-type strain sensor utilizing electric capacitive change. Wireless measurements are done using amplitude modulation. These sensors are used to measure the strain of tires in-service to improve reliability of tires and ABS systems. The advantage of this sensor to conventional strain gauges is their flexibility and wireless ability.

A **magnetic-based sensor** makes use of a magnetoelastic material which is subject to change in magnetic permeability when exposed to a strain or pressure [17]. This phenomenon is known as the Villari effect. A second approach in designing a touch sensor based on magnetic transduction is using the Hall effect for which the Hall voltage is a function of the flux density. The flux density measured at a point will change as an applied force causes a magnet to move. DiLella *et al*. [18] proposes a micromachined magnetic-field sensor that is based on an electron tunneling transducer. This tunnel sensor is very small, sensitive, requires very little power and operates at ambient temperatures. The sensors are fabricated by hot embossing replication with silicon templates, a fast, simple and repeatable method which makes this sensor a promising prospect for microsensing applications.

Optical-based sensors are also commonly used because of their small size and the fact that no electrical power is needed at the remote location. It uses the phenomena of photoelasticity. A force applied to a photoelastic material while light passes through it causes the plane of polarization to rotate which results in a change in light intensity which can be measured. Trpkovski *et al*. [19] demonstrated a dual temperature-strain point sensor by combining a

short length erbium-doped fiber in close proximity to a fiber Bragg grating. By measuring the green fluorescence intensity ratio in erbium and the Bragg wavelength shift, the temperature and strain can be deduced. Stomeo *et al*. [20] proposes the simulation and fabrication of a photonic crystal strain-sensitive structure. This shows that the optical properties of a photonic crystal can be used to fabricate sensors which are small in size and have good resolution.

Piezoelectric sensors work on the phenomenon of piezoelectricity, which is the ability of certain materials to generate an electric charge when subjected to an external mechanical stress. Materials that exhibit this property are usually crystals and some ceramics, but polymers such as polyvinylidene fluoride (PVDF) are normally used in sensors.

A **strain gauge** detects the change in length of a material it is attached to when the material is subjected to an external force. Mounting a strain gauge on a material and measuring the change of length of the strain gauge gives an indication of the magnitude of an applied force. A typical strain gauge is manufactured from either a resistive element or a semiconductor material.

A **force sensing resistor** (FSR) is a piezoresistive conductive polymer. Application of a force to the surface of a FSR will result in resistance in a predictable manner. It is normally supplied as a polymer sheet which has had the sensing film applied by screen printing.

Although these sensors can be compact, accurate and easy to fabricate, some applications require sensors to be bio-compatible and have certain properties.

3.2.2 Tactile sensing for biomedical applications

Medical Tactile Inc (MTI), an emerging medical device manufacturer located in Los Angeles USA, has developed a broad-based breast cancer diagnostic device called SureTouch [2]. MTI was the first to announce their palpation device for the clinical breast exam, but all around the world, Universities and companies are working on methods to reproduce the sense of human touch.

The SureTouch Visual Mapping system consists of a handheld device including a transducer with a footprint of about 30 mm by 40 mm. The transducer has almost 200 very small sensors able to record the pressure and location data. Each sensor individually measures the firmness of the breast underneath. As the patient is examined, a real time display of the palpable area is

digitally recorded. The data is converted to two-dimensional and three-dimensional formats depicting the size, shape, hardness, homogeneity and location of the lesion. Figure 2 shows the SureTouch Visual Mapping System.

Where the SureTouch Visual Mapping System senses pressure and hardness, Engel *et al*. [21] proposes a tactile sensing skin capable of evaluating contact forces, film curvature, relative hardness, thermal conductivity, and temperature of the contacted object.

Figure 2: SureTouch Visual Mapping System [2]

There is a common belief that in the near future, robotics will replace or serve as extensions of humans in dangerous, delicate, or remote applications. In order for robotics to achieve this, they must have sensory input similar or superior to that of human senses. Engel *et al*. [21] argues that "one of the most important senses for performing varied complex and precise tasks autonomously or remotely is the sense of touch". Tactile feedback from the human skin provides a multitude of information, including force, temperature, hardness, texture, and thermal conductivity [22]. This was the driving force behind Engel *et al*. to develop a multi-modal sensing skin.

Their device consists of four distinct sensors in each sensory node. These sensory nodes are arranged in an array to form the "skin". The four sections in each node incorporate the reference temperature sensor, thermal conductivity sensor and the contact force and hardness sensors. Sensing is accomplished through a nickel RTD (Resistance Temperature Device) for

temperature measurement and compensation; a gold heater and nickel RTD pair for thermal conductivity measurement; a membrane NiCr strain gauge based contact force and hardness sensor; and a reference contact hardness sensor. Figure 3 a) shows a single sensory node and Figure 3 b) shows an array of these nodes forming the skin.

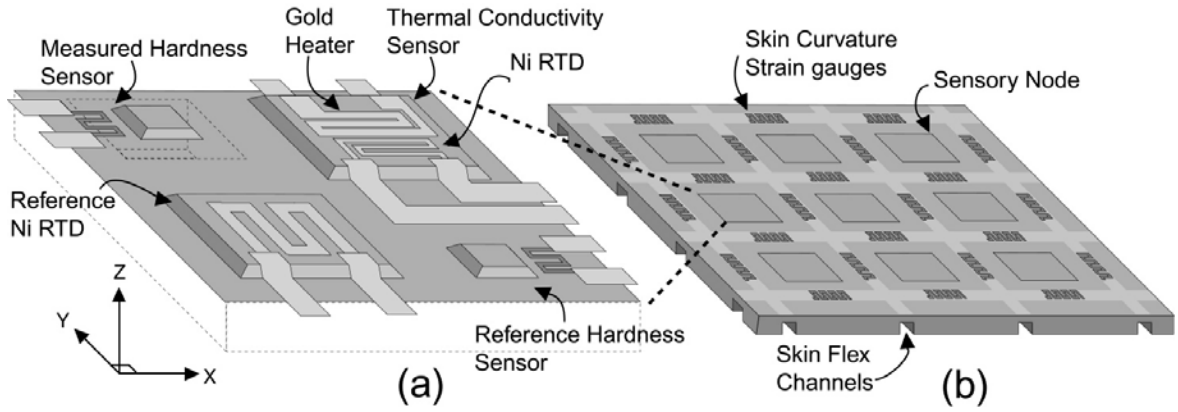

Figure 3: a) Sensory node, b) Skin [21]

The device is fabricated on DuPont Kapton HN200 2 mm thick polyimide film, which ensures flexibility, robustness, and a low material cost. Figure 4 shows a micrograph of the hardness sensor with NiCr strain gauge and of the reference bulk sensor illustrating the small size. At 100 μm across these sensors form a good substitute for human touch which has a spatial resolution of 0.5 mm according to Stramm [23]. Although this multi-modal sensing skin of Engel *et al*. fulfills all the requirements to represent the sense of touch, it is too expensive for the device proposed by this study.

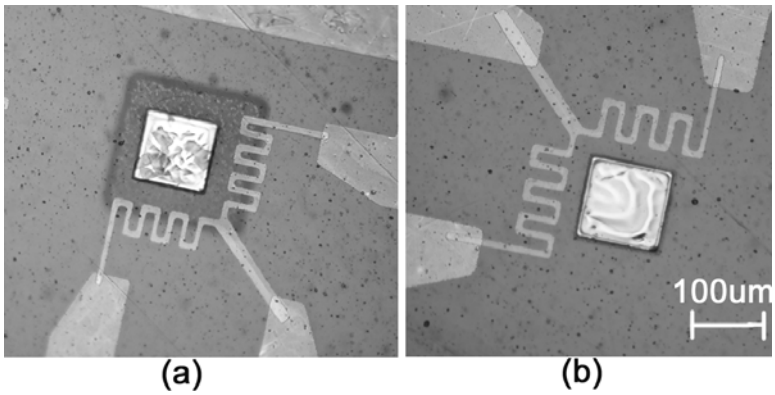

Figure 4: Micrograph of a) membrane hardness sensor and b) reference bulk sensor [21]

For the purposes of a neck palpation device, the emphasis will be on the pressure/force distribution of the sensed area. Daniel Stramm investigated tactile sensors which can be used

for medical examination at the human neck. According to Stramm [23], the human finger tip senses pressure, vibration and acceleration of the skin, and combining these gives the tactile sensation with a spatial resolution of 0.5 mm.

Stramm [24] investigated numerous pressure sensors available on the market as well as concepts of his own. The concept he did further work on involved pins pressing against the skin with the ends of the pins displaying the surface of the skin. This is scanned by a 3D scanner and displayed on a computer screen in real-time.

A more promising concept he investigated is the use of piezoresistive pressure sensors forming a tactile sensing array. This is done by linking several of these piezo resistive sensors together in a certain array. The pressure sensed by each sensor can be calculated and used to create a map of the neck area showing areas where a firmer mass exists. The advantage of piezo resistive pressure sensors are their low cost and good spatial resolution.

Kane [25] argues that the spacing of the papillary ridges of the human dermis is 300 μm. He further describes the first large-area tactile sensing array capable of measuring axial and shear contact stress profiles at the same spatial resolution. The array consist of 4096 (64 x 64) sensors and is fabricated using VLSI circuit fabrication techniques.

Howe and Cutkosky [26] present a scheme that can detect the onset of slip on a surface as well as detect various parameters of surface texture. Basu *et al*. [27] and Buttazzo *et al*. [28] also propose methods to determine surface texture using tactile sensing. Fearing and Binford [29] proposes a cylindrical sensor capable of determining principal curvatures, normal forces and location. Russel and Parkinson [30] describe the design and construction of a tactile sensor capable of measuring the surface shape of an object being held between the fingers of a robot gripper.

Berger and Hess [31] investigated the use of FSRs as tactile sensors for medical examination at the human neck. They tested FSRs for repeatability, time stability and they determined the characteristic graphs of the FSRs. They found the error of repeatability to be under 10% and that the values do not change significantly over time.

The characteristic curve of the individual sensors does not vary much and a mean curve was constructed using the mean values of four randomly chosen sensors. The characteristic curves

of these sensors as well as the mean curve were calculated and plotted using Matlab and are shown in Figure 5.

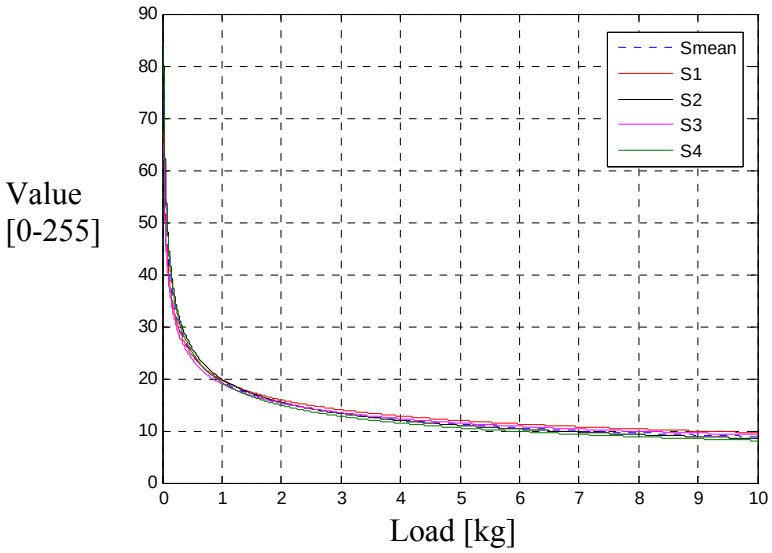

Figure 5: Characteristic curve of FSRs

This mean curve will be used to determine the load a sensor is experiencing. Figure 6 shows the percentage error of using the mean curve as opposed to the individual sensor's characteristic curve. It is clearly evident that the percentage error using the mean curve is negligible for loads higher than 0.1 kg.

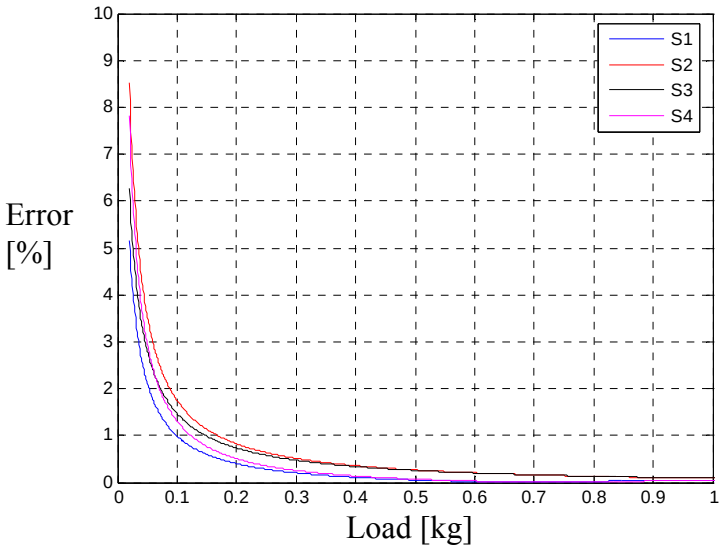

Figure 6: Error by using mean curve

One big disadvantage of the FSRs is their large spatial resolution. Each FSR's sensing area is ~ Ø 8 mm. In order to improve the resolution a technique known as image registration was used.

3.3 IMAGE REGISTRATION

Digital image registration is a branch of computer vision that deals with the geometric alignment of a set of images [32]. This set of images can be two or more images taken of a specific object at different times, from different viewpoints or by different sensors. The goal of image registration is to geometrically align these images into a common reference frame. Image registration is usually necessary in image analysis tasks which integrates information obtained from a combination of data sources. This is the case for image fusion, change detection, multi-channel image restoration, and for modal-based object recognition.

A lot of work has been done in the field of image registration because of its importance in remote sensing, medical imaging, computer graphics, and computer vision. Some of the more common registration tasks include image mosaics, weather forecasting, topographic mapping, creating super-resolution images and multi sensor image fusion. In medicine it is used to combine computer tomography (CT) and NMR data for more complete information, monitoring tumour growth and comparing of patient's data with anatomical atlases [32-33]. Figure 7 shows an image before and after registration, in this case the task was to create a super-resolution image. Super-resolution refers to an image registration technique used to improve the resolution of an image using multiple images of the same thing from different viewpoints. Using multiple images it is possible to combine these images and improve the resolution of an image significantly as is shown in Figure 7.

Figure 7: Creating a super-resolution image using registration [34]

In the case of the neck palpation device, image registration will be used for creating a better resolution image from the images sensed by the FSRs. The image sensed by the FSRs refers to an array of measurements of the FSRs. Each pixel corresponds to the measurement of the

pressure sensed by a FSR. The image registration technique should be used irrespective of arbitrary translations and rotation angles of the various images. In order to tackle this problem knowledge on different image registration methods should be gathered.

Brown [35] introduced a framework in which all registration techniques can be understood and consists of the following four components:

1. **Feature space** – extracts the information in the images that will be used for matching.
2. **Search space** – the class of transformations, or deformation models, that is capable of aligning the images.
3. **Search strategy** – decides how to choose the next transformation from this space, to be tested in search for the optimal transformation.
4. **Similarity metric** – determines the relative merit for each test. The search continues according to the search strategy until a transformation is found whose similarity measures are satisfactory.

Image registration can be seen as a mapping between two images with respect to transformation and intensity. We can define these images as two 2D arrays $I_1(x,y)$ and $I_2(u,v)$, with I_1 the reference image. The mapping between the two images can then be expressed as:

$$I_1(x,y) = g(I_2(f(u,v))). \tag{1}$$

Where f is a 2D spatial-coordinate transformation operator that relates the (u,v) coordinates in I_2 to the (x,y) coordinates in I_1, and g is the 1D intensity function. The registration problem now becomes one of finding the optimal spatial and intensity transformations so that the images are matched. The intensity transformation, g, is not always necessary but is useful when images taken from different sensors are registered. Often a simple lookup table of the sensor's calibration data is sufficient to estimate g.

Finding the optimal spatial or geometric transformation parameters now becomes the key to the registration problem. It is usually expressed as two single-valued functions:

$$I_1(x,y) = I_2(f_x(u,v), f_y(u,v)). \tag{2}$$

A couple of different techniques will now be discussed which can be used to solve the optimum spatial transformation.

3.3.1 Non-linear Least Squares Optimization using LMA

One of the most commonly used techniques uses the standard Levenberg-Marquardt algorithm (LMA) that makes use of a non-linear least squares optimization technique. The LMA is commonly used in image registration [32], motion estimates [36], image mosaics [37-38] and video-indexing. The LMA makes use of a zero-mean normalized sum of squared differences (SSD) as the similarity measure between the two images:

$$\begin{aligned}\chi^2(a) &= \int_{xCR^2}\int\left(I_1(x) - I_2{}'(x)\right)^2 dx \\ &= \int_{xCR^2}\int\left(I_1(x) - I_2(f(u))\right)^2 dx \\ &= \left\|I_1(x) - I_2(f(u))\right\|^2.\end{aligned} \tag{3}$$

and in discrete form this becomes

$$\chi^2(a) = \sum_{i=1}^{N}\left[I_1(x_i) - I_2(f(u_i))\right]^2. \tag{4}$$

In this equation f is the spatial transformation matrix of size 3 x 3 applied to image I_2 to map it from its *(u,v)* coordinates to the *(x,y)* coordinates of I_1. The LMA optimize the parameters *a* of the model curve $f(u_i|a)$ to minimize χ^2. An initial guess of the parameter vector *a* is required. In each iteration step, the parameter vector *a* is replaced by a new estimate $a+q$. To determine *q,* the functions $f(a+q)$ are approximated by their linearizations:

$$F(a+q) \approx f(a) + Jq. \tag{5}$$

where *J* is the Jacobian of *f* at *a*.

3.3.2 Log-Polar transformation

Log-polar transformation makes use of polar mapping and logarithmic scaling which results in it being non-linear and non-uniform. Define the coordinate system *(log r, θ)* where r is the radial distance from the center (x_c,y_c) and θ denotes the angle. Any point *(x,y)* can be represented by

$$\begin{aligned} r &= \log\sqrt{(x-x_c)^2 + (y-y_c)^2} \\ \theta &= \tan^{-1}\left(\frac{y-y_c}{x-x_c}\right). \end{aligned} \tag{6}$$

Applying such a polar coordinate transformation to an image will map radial lines in the Cartesian system to horizontal lines in the new polar coordinate system. Figure 8 a) shows an image I that was mapped to an image $I_{r\theta}$ in Figure 8 b) using this log-polar transformation. Note that r lies along the horizontal axes and θ lies along the vertical axes.

The log-polar transformation has two distinct advantages, rotation and scale invariance; and spatial varying sampling which has a higher resolution near the focus point and thus reduces the amount of information. This makes it possible to process a high resolution image only at a certain focus location while being aware of a wider field of view. This phenomenon is also present in the retina of a primate and is an accepted model of the representation of the retina [39].

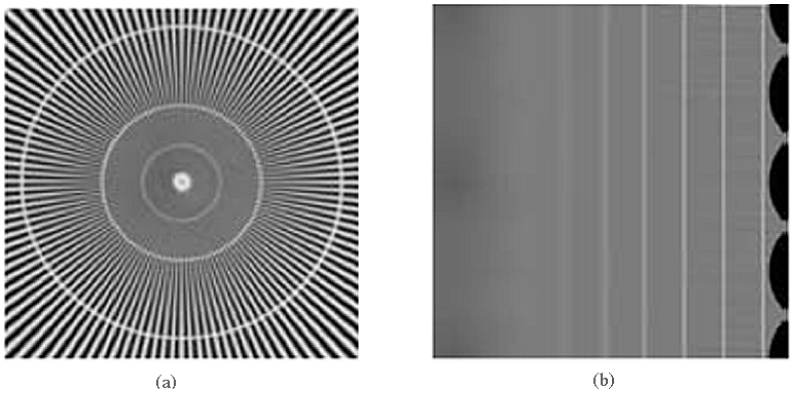

Figure 8: Log-polar transformation, a) input image I b) transformed image $I_{r\theta}$ [32]

3.3.3 Feature based image registration

Feature-based image registration algorithms extract certain salient structures from graylevel images. These structures are used to establish correspondence between the two images. The structures that are extracted can be points, lines, curves or any region on the images. Finding these features is an important part in the technique and there are several methods proposed to do this. Schaffalitzky and Zisserman [40] detect quadrilateral and elliptical regions which they use as their extracted structures. These regions are used to find the fundamental matrix in wide-baseline stereo images. Tuytelaars and Gool [41] look for locally affine regions where they compute several degrees of moments to build feature vectors for image retrieval.

Feature-based image registration algorithms are very complex and they need clearly defined structures to extract and use. The images produced by the neck palpation device are of very poor resolution and don't have clear and repeatable structures to extract.

3.3.4 Fourier- Mellin transform

Simple phase correlation can be used to map the translation between two images. The Fourier-Mellin transform extends the phase correlation to include rotation with properties of Fourier analysis [42-43]. According to the properties of the Fourier transform relating to translation and rotation, the images are related by

$$\begin{aligned} I_1(x,y) &= I_2\left(f_x(u,v), f_y(u,v)\right) \\ u &= x\cos\theta + y\sin\theta + tx \\ v &= -x\sin\theta + y\cos\theta + ty. \end{aligned} \tag{7}$$

A Fourier transform transforms a function *f(m,n)* with two spatial variables *m* and *n* to:

$$F(\omega_1,\omega_2) = \sum_{m=-\infty}^{\infty}\sum_{n=-\infty}^{\infty} f(m,n)e^{-j\omega_1 m}e^{-j\omega_2 n}. \tag{8}$$

where ω_1 and ω_2 are frequency variables. Applying the Fourier transform to equation (7) gives:

$$\begin{aligned} F_1(\omega_x,\omega_y) &= F_2(\omega_u,\omega_v)e^{-j(\omega_x x_0 + \omega_y y_0)} \\ \omega_u &= \omega_x\cos\theta + \omega_y\sin\theta \\ \omega_v &= -\omega_x\sin\theta + \omega_y\cos\theta. \end{aligned} \tag{9}$$

It should be noted that the magnitude spectra $|F_1|$ is a rotated replica of $|F_2|$, both spectra share the same center of rotation. This rotation can be recovered by representing the spectra $|F_1|$ and $|F_2|$ in polar coordinates:

$$|F_1(r,\theta)| = |F_2(r,\theta-\theta_0)|. \tag{10}$$

The Fourier magnitude in polar coordinates differs only by translation. The phase-correlation method can be used to find this translation and estimate θ_0.

According to [33] investigation has shown that rotation and scaling introduce aliasing in low frequencies at the borders. They suggested a two step process to alleviate the aliasing problem. First the image must be multiplied by a 2-D radial mask and secondly a low-pass filter must be applied to remove the offending low frequencies. Another problem presents itself when the sensed image differs from the reference image with respect to scale. This though will not affect the images measured by the neck palpation device as there are no

magnifications and the sensed image is always a translated and rotated version of the reference image.

3.3.5 Multiresolution Pyramid

The multiresolution pyramid method is an improved version of the LMA method described in Section 3.3.1. It consists of a set of images in multiple resolutions representing one image. The original image is at the base of the pyramid and is downsampled by a constant factor in each dimension to create the image at the next level. This is repeated until the tip of the pyramid is reached where the image size at the tip i is reduced from the original by a factor of 2^i in each dimension. This tip of the pyramid is known as the coarse level while the base of the pyramid is known as the finest level.

The LMA method is now applied at the coarsest level which has a hugely reduced number of pixels thus enhancing the computational time. Secondly, a smoothness condition appears due to limits imposed on the levels causing χ^2 *(a)* to be computed on smoother images. Figure 9 shows the interpolation from the coarse grid to a finer grid.

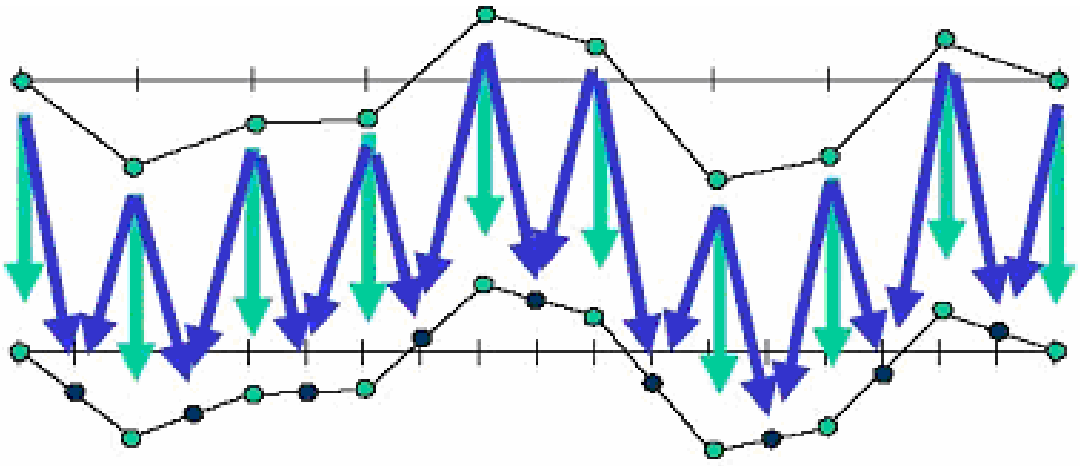

Figure 9: Interpolating from the coarse grid to a finer grid [32]

The coarsest level only retains large scale features and progresses from the coarse level to finer levels where smaller features are integrated. The parameters must be scaled properly across these different levels and usually uses a simple scale factor.

The important steps in the method are:

1. **Smoothing**. Reducing high frequency errors by using few iterations of the LMA method.

2. **Restriction**. Downsampling the residual error to a coarser grid.

3. **Prolongation**. Interpolating a correction computed on a coarser grid into a finer grid.

There are other different modifications to the LMA method and the log-polar methods described by Zokai and Wolberg [32]. These methods though are used to minimize computation time by eliminating iteration steps etc. The image from the sensor developed in this study is a 5x5 matrix and the computation time is therefore not such a big concern.

The algorithm developed for the purpose of improving the resolution of the image captured with the FSRs will now be discussed.

4. SUPER RESOLUTION ALGORITHM

For the purpose of this study the feature space will be an array of the measured pressure by the FSRs. Simple rotation and translation properties as described in Section 3.3.4 is used to transform the coordinate system of an image I_2 to that of a reference image I_1. This is the Search space. Figure 10 shows this transformation.

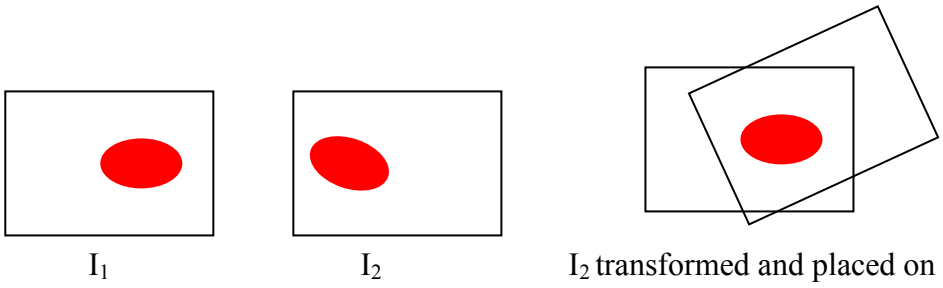

Figure 10: Translation and rotation transform

Each pixel in the matrix has a unique number associated with it according to its x and y coordinate, eg. the uppermost left hand pixel is (0,0) and the lowermost right hand pixel is (4,4) for a 5x5 matrix. The pixels in I_2 need new indices to let the red oval correspond with the red oval in I_1. Thus each pixel undergoes the transformation for both the x and y coordinate.

$$u = x\cos\theta + y\sin\theta + tx$$
$$v = -x\sin\theta + y\cos\theta + ty$$

The parameters that can be adjusted are tx, ty and θ. After a first step the two images are compared by calculating $\chi^2\ (a)$ using equation (4). This step simply subtracts the two images from each other, takes the square and sums all the different elements in the matrix. This produces a single number indicating how well these two images were aligned. A simple Powell optimization technique is used to minimize the number $\chi^2\ (a)$ which is the similarity metric.

The optimization technique adjusts tx, ty and θ each time and is the search strategy. The search strategy produces a new $\chi^2\ (a)$ after each iteration. This process repeats itself until $\chi^2(a)$ is minimized below a pre-described value.

For the purpose of this study 25 images will be registered and combined together using the above-mentioned technique. 25 images are used because it was suggested by Stefan van der Walt to use between 20 and 30 images for the registration algorithm. Stefan van der Walt is

currently doing his PhD in image registration at the University of Stellenbosch. It was found during the test phase that using more than 25 images becomes redundant and does not affect the outcome much.

Before the algorithm is reached though, each image is scaled with normal linear interpolation to a 17x17 matrix and it is normalized so that the maximum value in each matrix is 1. The algorithm and other techniques used will be discussed in more detail in the computer code Section 6.6.

In the next section the two concepts considered for the device will be described.

5. ENGINEERING SPECIFICATIONS AND CONCEPTS

In this section the goal was to generate engineering specifications for the device. This will give a clearer understanding of the problem and will show exactly what needs to be designed. The engineering specifications follows from customers' requirements and these are discussed in the first section. Other detection methods used are compared against the customers' requirements and engineering specifications in a House of Quality [44]. The House of quality is a tool used to generate specifications or goals and see how competition meets these goals. It also gives numerical targets to work towards and gives an indication where improvements can be made on existing products.

Using the engineering specifications and the results of the House of Quality, the function of the prototype is stated and decomposed after which the concepts are discussed.

5.1 REQUIREMENTS AND SPECIFICATIONS

Engineering specifications are an important part in any design process. It sets clear targets to work towards in order to satisfy the customers' requirements. In order to generate the specifications though, it is necessary to understand exactly what the requirements are. The requirements of the device refer to what the customers want or expect from the device. Here the customer is the patient as well as the doctor and any other person involved in the life cycle of the device. This will include the maintenance person as well as the operator.

The main goal of the study is to develop a prototype of a neck palpation device to assist a medical practitioner. The device is aimed at telemedicine environments, rural areas where doctors are scarce. The device will aid in initial examination performed by a trained operator. The data gathered must emulate the data a doctor will acquire during manual palpation. The data must be saved in an electronic format that can be sent to a doctor to make a diagnosis or suggest further examination. Keeping the problem statement and different customers in mind the customer's requirements can be listed.

As this study was not intended for clinical tests, the study was not performed in conjunction with a medical practitioner. The requirements listed in Table 2 are therefore not provided by

any person involved in the life cycle of the device and is merely the result of an individual brainstorming session.

Table 2: Customers' requirements

	Requirements
1	Reliability
2	Repeatability
3	Safe to use
4	Comfortable
5	Easy to use
6	Easy to maintain
7	Robust and durable
8	Cost effective
9	Easy to manufacture
10	Scan and distinguish different sized lymph nodes

Before such a device can be used for clinical testing it would need to conform to certain standards. These were not considered as the device was never intended for clinical trials.

The next step is to develop a set of engineering specifications from the customers' requirements listed in Table 2. Specifications are an explicit set of requirements to be satisfied by a product. In other words, the specifications are a restatement of the design problem in terms of parameters that can be measured and have target values. This will give an indication of how well the device satisfies the customers' requirements. It is important to generate parameters for each customer requirement. Table 3 List the specifications.

Another requirement not listed in Table 3 is the use of FSRs. FSRs were chosen because of their availability and ease of use. The only disadvantage of using FSRs when considering the engineering specifications is the high resolution of the FSRs. The resolution is greater than the 5mm target.

Table 3: Engineering Specifications

	Specifications	Target (disgusted)	Target (delighted)
1	Energy required	High	Low (200 W)
2	Number of Standard parts	500+	3-
3	Examination time	20+ min	5- min
4	Resolution	5+ mm	0.3- mm [7-9]
5	Required access	Whole body	12 cm² [7]
6	Safety	Unsafe	Very Safe [7]
7	Cost	Very High	Low [7-8]
8	Portability	Large and not portable	Small and portable [7]

To understand the problem at hand clearly it is necessary to break the problem down into its fundamental functions. This is done in the following section.

5.2 FUNCTIONAL DECOMPOSITION

Before concepts are generated, the function needs to be understood. A technique known as functional decomposition is used [44]. The function of the device refers to what the device does and not how it is done. Dividing the overall function into finer functional detail or sub-functions, lead to a better understanding of the problem. The functional decomposition for the neck palpation device is shown in figure 11.

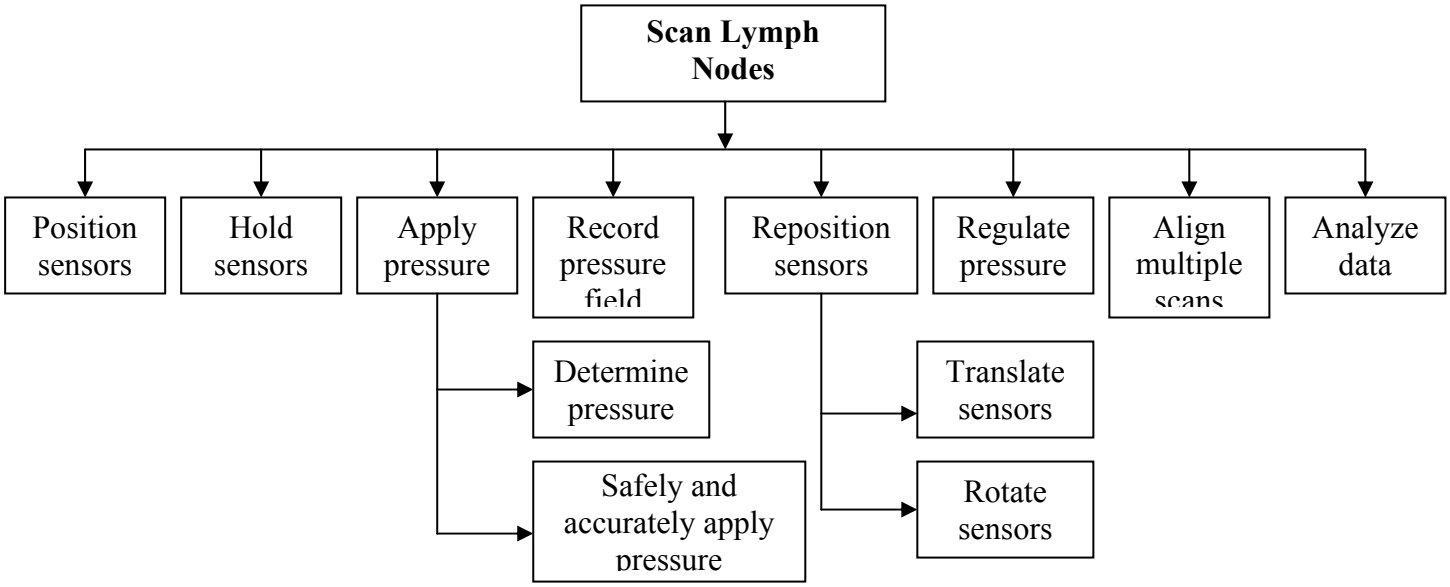

Figure 11: Functional decomposition

Once the function of the device is fully understood the House of Quality is used to compare existing detection devices.

5.3 HOUSE OF QUALITY

Figure 12 shows the House of Quality or Quality Function Deployment (QFD) as described by Ullman [44] for the four concepts. The QFD method is designed to develop and organize the major pieces of information necessary to understand the engineering problem:

- The specifications of the product
- How the different concepts and competition meets the goals
- What is important according to the customers
- Numerical targets to work toward

The top left hand block indicates all the customers. This will include the patient as well as the operator, doctor and maintenance person. The larger block to the right is the customer block and just beneath it is the “what” block. This block indicates the customer’s requirements. These requirements are then weighted in importance for each customer in the block directly below the customer block. The block with the roof indicates the engineering specification for the requirements and this is compared to the requirements in the big block in the middle. The specifications and requirements are compared in terms of the relationships that exist between any two of them. The block at the bottom identifies the engineering targets for the specifications. Lastly the block at the right evaluates the concepts against the requirements from bad (1) to good (5).

S = strong relationship
M = medium relationship
W = weak relationship
Blank = no relationship

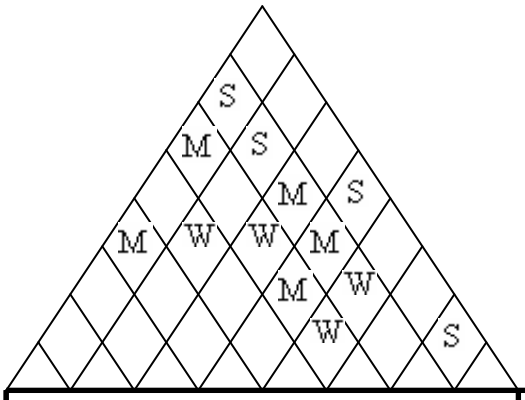

WHO				HOW								NOW
Operator	Doctor	Patient	Maintenance person	Energy required	Non Standard parts	Resolution	Required access	Safety	Time per examination	Cost	Portability	U=Ultrasound C=CT M=MRI P=PET H=Hand held
				WHAT	**WHAT vs HOW**							**Now vs What**
				Units	W	#	mm	mm	y/n	min	R	y/n	1 2 3 4 5
5	20	8	15	Reliability			S						HUCMP
10	20	8	5	Repeatability			M			W		W	H UCMP
10	5	20	3	Must be Safe			M						CP H U M
4	5	20	3	Comfortable					W		W		P CM UH
20	3	3	5	Easy to use			M						PMCUH
4	3	3	20	Easy to maintain		S	M						M PC UH
10	3	3	15	Robust and durable			M						M PC U H
8	10	5	10	Cost effective	S	S	S						M PC U H
4	5	3	15	Easy to manufacture		S	S	S					M PC U H
15	8	10	3	Distinguish sizes									CMPUH
				HOW MUCH									
				Hand held	low	3	1	15	y	5	low	y	
				Ultrasound	low	20	0.3	15	y	5	low	y	
				CT	high	999	1	999	n	10	hgih	n	
				MRI	high	999	1	999	y	15	high	n	
				PET	high	999	1	999	n	60	high	n	
				Target (delighted)	low	3	0.3	20	y	5	low	y	
				Target (disgusted)	high	500	5	999	n	20	high	n	

Figure 12: House of Quality (QFD)

Figure 12 helps to understand the problem better. The key requirements and engineering specifications are clear and it is also visible to see how well the other methods of detection satisfy the specification. This understanding of the problem is used as a basis for generating concepts. It is clear that CT, MRI and PET have a lot of disadvantages for use in telemedicine environments. Taking Figure 11 and Figure 12 into account, different concepts were generated and evaluated. The main two concepts will now be discussed.

5.4 HAND HELD TRANSDUCER

The first concept considered was the hand held transducer which is similar to the SureTouch Visual Mapping System [2]. This is quite a common type of device and studies have been done using such a device by Kaufman [6], [45] and Ables *et al.* [46-47] for breast mass screening.

This device is a small hand held device with a footprint of about 3 cm by 4 cm. On the footplate of the device are hundreds of tiny pressure sensors. The SureTouch system [2] makes use of capacitive based pressure sensors but for this study FSRs was proposed because of their availability, ease of use and cost. The SureTouch system records a real time display of the sensed area which is then converted to a colour image. This image consists of a 2-D and 3-D representation of the sensed area depicting the shape, size and hardness. According to Kaufman [45], the device correctly identified 94% of masses during a breast examination study compared to the 86% by physical examination. The device also gives a reproducible record which allows for objective review by various examiners.

Using FSRs, only about 25 sensors (5x5) can be fitted on the footplate. The footplate of this device is placed over the location of the neck. The FSRs each measures the force (firmness) of the part of the neck directly underneath them. The operator of the device needs to apply the necessary pressure.

The device will be moved slightly to a new position to take a new measurement of the firmness of the neck beneath each sensor. This step will be repeated numerous times until enough information is acquired. The operator must exert the necessary pressure on the device at each new position. The information gathered is then sent to the image registration algorithm

which will generate a final image of the sensed area. The shape, size and hardness will be illustrated in the final record. Figure 13 shows a concept drawing of the proposed device.

An advantage of this device is the simplicity of the design which relates to ease of manufacturing and low cost. The device is robust and will be easy to maintain as there are no movable parts. The only big disadvantages or limitations are due to operator issues. The operator requires training to properly use the device and the device won't always exert the same pressure on the neck as this will vary between operators. Due to this the results obtained can rely relies greatly on the operator which is not ideal. Most of the other detection methods such as CT or MRI do not rely on the operator as the apparatus does all the work and no hman interaction is necessary.

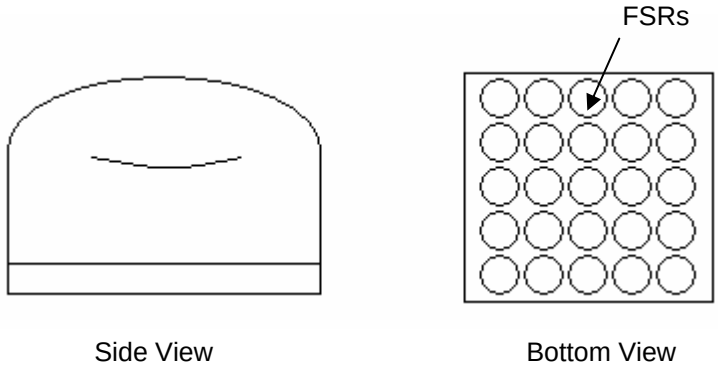

Figure 13: Hand held transducer

5.5 INFLATABLE BLADDER

The second concept consists of a neck brace and an inflatable bladder mounted in the inside of the brace. The pressure sensors are mounted in an array on the surface of this inflatable bladder. The bladder is connected to a small air pump and a release valve for safety. The neck brace will be fitted around a patient's neck. As the bladder is inflated the sensors presses against the patient's neck and the sensors can measure the firmness of the tissue below. Figure 14 shows a top view of the concept.

The inflatable bladder eliminates the need for a trained operator as is the case for the hand held transducer. The pressure exerted by the bladder can be controlled and more importantly it can repeatedly be inflated to precisely the same pressure. This increases the repeatability of all examinations. The concept is also simple and easy to manufacture using standard parts.

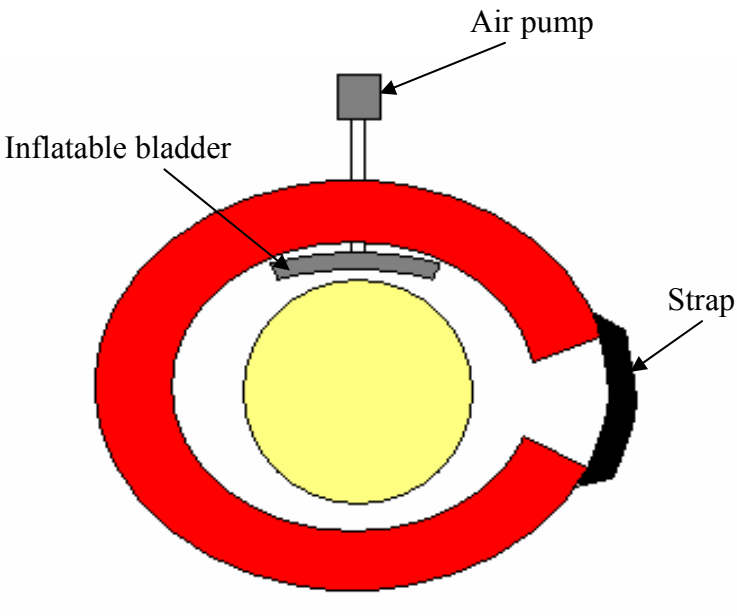

Figure 14: Inflatable bladder

A disadvantage is again the problem to move the bladder to numerous positions. This can be dealt with by just slightly rotating and moving the neck brace. Another alternative to accomplish this will be explained in the detail design section as this concept was deemed to be the winner.

Comparing the two concepts and looking at the engineering specifications it was decided to develop the inflatable bladder concept further. They are easy to use, cost effective and easy to manufacture. The main advantage of the inflatable bladder concept is the fact that the pressure can be accurately controlled. This ensures that the pressure at which the sensors are pressed against the neck will stay the same for all tests and this would improve repeatability and accuracy of results. The concept will now be discussed in detail.

6. DETAIL DESIGN

As mentioned in the previous chapter, the concept chosen to design and develop is the inflatable bladder concept. In the detail design section the concept will be developed into a working prototype. To add some structure to this chapter it will be divided into four sections:

1. Detail description of design
2. System layout
3. Individual components
4. Computer code

6.1 DETAIL DESCRIPTION

A short description of the concept was given in the previous chapter. Here a more detailed description will be given. Figure 15 shows a picture of the final prototype.

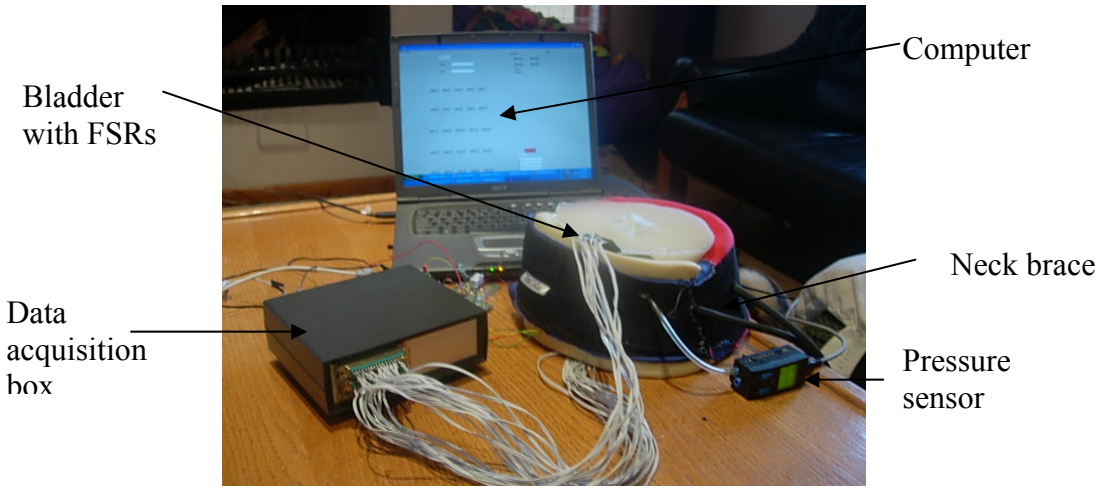

Figure 15: Final prototype

All the different parts of the design can be seen in Figure 15. A trained nurse or operator will put the neck brace around the patient's neck. The neck brace is ergonomically designed and will fit most people comfortably. The brace is then fastened with the two clicking straps at the back. The bladder will now be neatly positioned against the patient's neck in the area where the anterior and posterior lymph nodes are located. These are the two large groups of lymph nodes together with the submandibular nodes.

The pump and valve are neatly positioned into the neck brace. Two holes were cut into the foam of the neck brace using a heating element. Figure 16 shows the pump and valve.

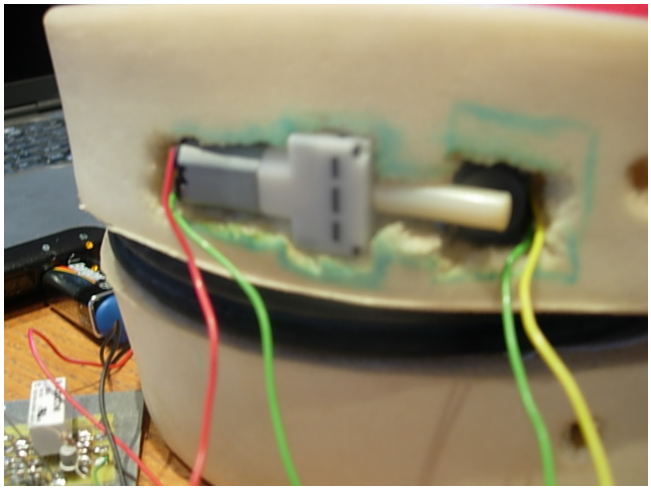

Figure 16: Location of pump and valve

The pump is connected to the computer's sound port through a control circuit. The pump is controlled to a certain pressure using the computer's sound card. This will be discussed in more detail in Section 6.3.3. The operator chooses the pressure the system is going to operate at and this will cause the pump to inflate the bladder to the desired pressure. Pressure is given as mmHg.

25 FSRs forming a 5x5 matrix is mounted to the surface of the bladder. As the bladder inflates, the FSRs press against the desired location on the patient's neck. An FSR pressing against a harder object will have a lower resistance than one pressing against the softer tissue. This information is then sent to the data acquisition box. Each FSR is connected to the data acquisition box by means of two wires. The data acquisition box in turn is connected to the computer using either a USB or a serial port. Using the user friendly interface the operator indicates that the first measurement can be taken. Figure 17 shows the user interface.

The operator must now adjust the brace after each measurement is taken. This can be done manually by rotating or slightly moving the whole neck brace up or down. The neck brace can also be adjusted by squeezing the appropriate hand pump at the front of the neck brace slightly. This causes the upper half of the neck brace to move up slightly. This is achieved by an inflatable rubber bladder that separates the bottom half from the top half of the neck brace. This can be seen in Figure 18. As the bladder is inflated, it forces the two halves of the neck brace apart. The inflatable bladder containing the FSRs is attached to the upper part of the neck brace.

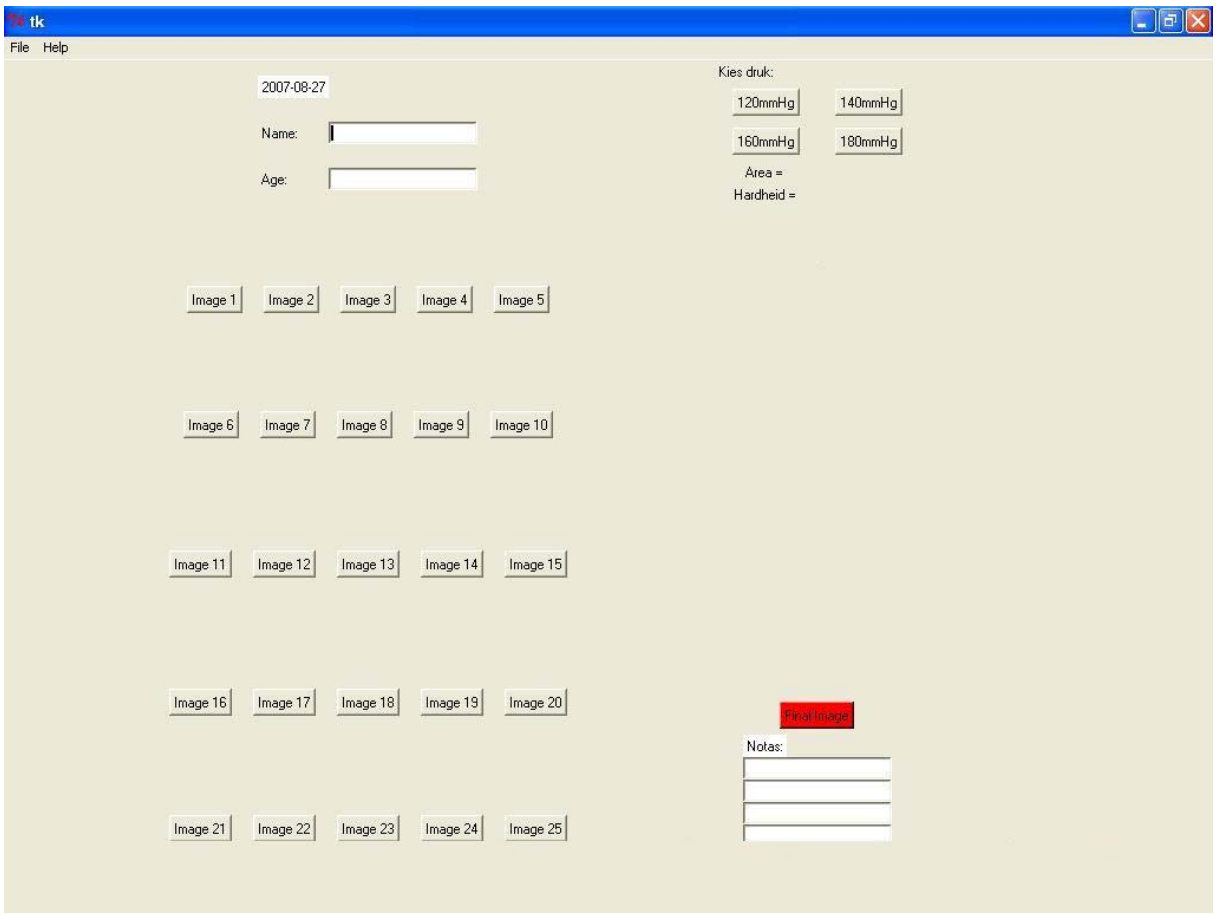

Figure 17: User interface

Figure 18: Two halves of neck brace

The user interface also allows the operator to include general information of the patient. There is also an area where the operator can add notes regarding the procedure or anything the operator thinks can be of value to the doctor.

The neck brace has to be adjusted 24 times for the 25 different images required. These are all displayed as individual images above the corresponding button. When all 25 images are recorded, the operator can press the final image button which will then send the images to the

image registration algorithm. Here the images are transformed and placed on top of each other in an effort to improve the resolution as was described in Chapter 3.3. The final image will show the shape of the sensed node as well as numbers giving an indication of the size and hardness.

The next section will explain the layout of the system.

6.2 SYSTEM LAYOUT

This section will describe the layout of the entire system i.e. what is connected to what, why and how. To better follow the reasoning a schematic of the layout is provided in Figure 19.

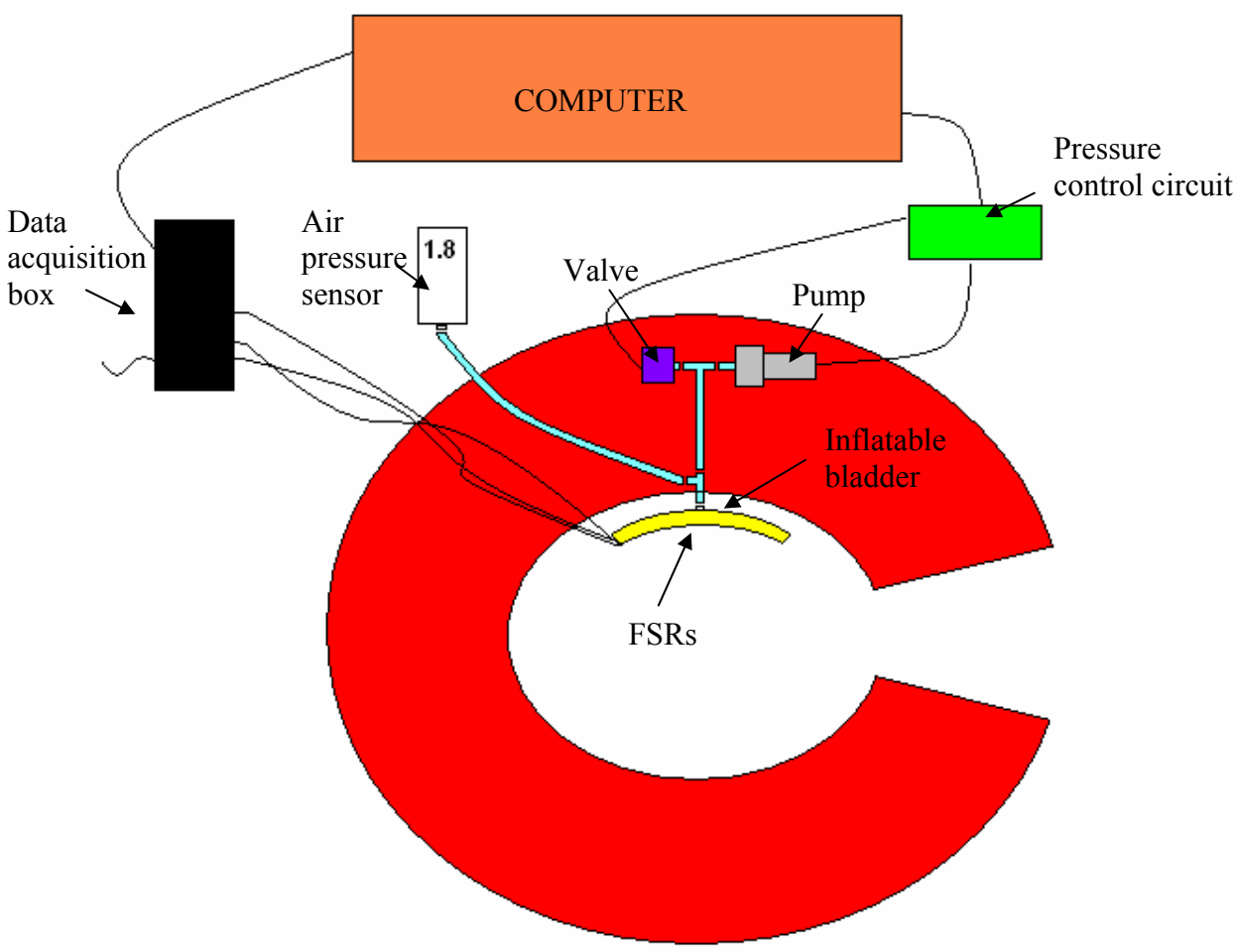

Figure 19: System layout

As can be seen in Figure 19, a computer is the main control unit of the system. The data acquisition box is connected to the computer via a USB port or a RS232 serial port. The connection at the data acquisition box is a RS232 serial port. The pressure control circuit is also connected to the computer with a normal headphones jack. This is plugged into the headphones/speaker socket of the computer.

The pressure control circuit is connected to the air pump and release valve by means of two wires for each (positive and negative). The circuit requires two 9 V batteries. The air pump and release valve fit nicely into the spaces provided for them in the neck brace. They are both connected to a 4 mm plastic tube through a T-piece. This connection is shown in Figure 20. The 4 mm tube sits in a hole cut through the neck brace using a heat element.

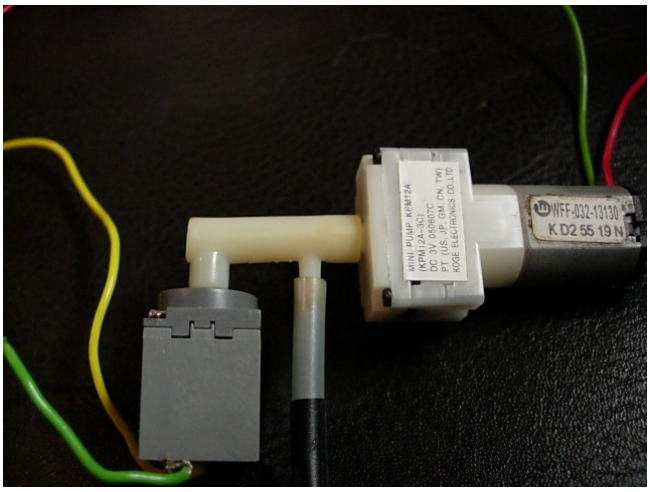

Figure 20: T-piece connection for pump and valve

The plastic tube was acquired from Festo while the T-piece, pump, valve and inflatable bladder was part of a wrist blood pressure monitor specifically bought to strip for the parts. At the end of the 4 mm tube is another T-piece. This T-piece connects the preceding components with the inflatable bladder and an air pressure sensor. This T-piece was also part of the blood pressure monitor and the one end of it is specifically designed to fit neatly into the bladder. The other end is connected to the pressure sensor via a 6 mm plastic tube. The air pressure sensor was also obtained from Festo. The T-piece connection is shown in Figure 21.

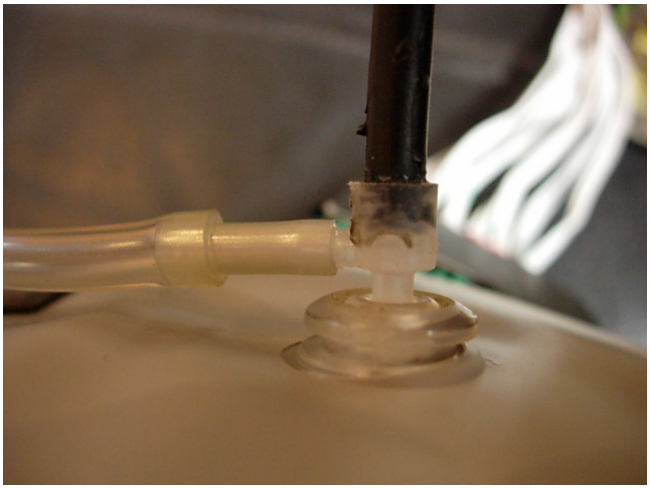

Figure 21: T-piece connection for bladder and pressure sensor

The air pressure sensor was originally bought to be used for feedback to the pressure control circuit, but as it turned out this was not possible as will become clear in the section on the control circuit.

The FSRs are each attached to the surface of the inflatable bladder using superglue and tape. Each sensor is then connected to the data acquisition box through two wires. This gives a total of 50 wires running from the surface of the bladder to the data acquisition box. This is shown in Figure 22.

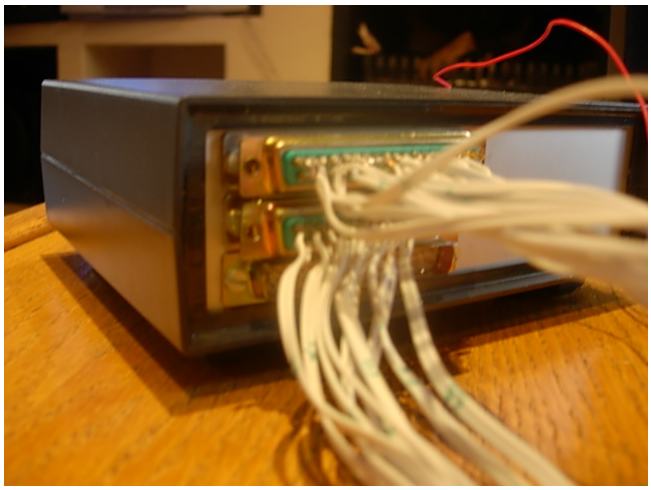

Figure 22: connection at the data acquisition box

Now that the working of the system and the system layout is clear, each individual component will be discussed in more detail.

6.3 DESCRIPTION OF INDIVIDUAL COMPONENTS

This section will describe the design and importance of the main components. The section will be divided into six parts discussing each component:

1. FSRs
2. Inflatable bladder
3. Pump, valve and control circuit
4. Data acquisition box
5. Air pressure sensor
6. Neck brace

6.3.1 FSRs

The pressure or force sensors used in this study are FSRs. 25 of these FSRs were attached to the inflatable bladder using superglue. Each FSR is roughly 6 mm wide and 40 mm long with the sensing area about 8 mm in diameter. Only the sensing areas of the FSRs were glued to the bladder and they were positioned as close to each other as possible forming 5 rows and 5 columns. This is shown in Figure 23.

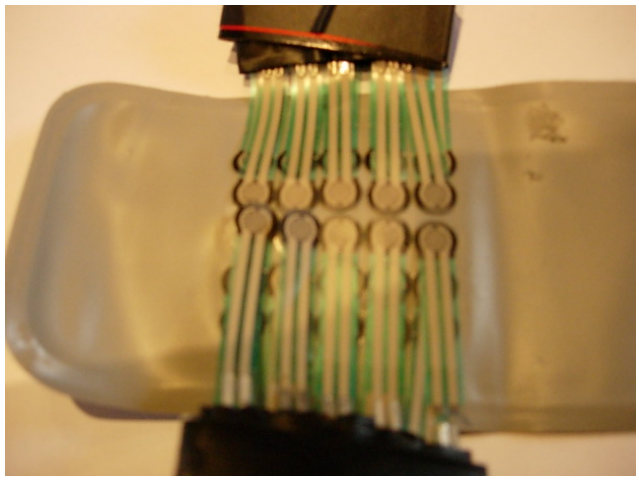

Figure 23: FSRs

FSRs are similar to strain gauges with the exception that FSRs are more flexible (they are made of a polymer) and they respond to a normal force instead of a longitudinal strain. FSRs also have a logarithmic response characteristic compared to the usual linear characteristic of strain gauges. This logarithmic characteristic enables FSRs to cover a larger range with good accuracy. Figure 24 shows this logarithmic response.

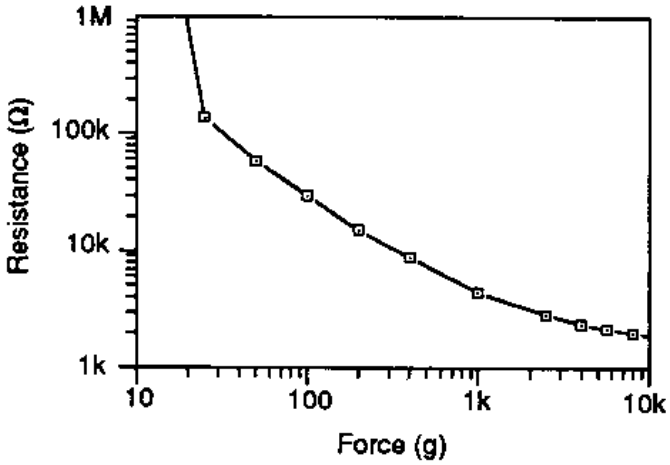

Figure 24: FSR characteristc curve [48]

Another attractive feature of the FSRs is that Tekscan [49] can create custom sensors of almost any size and shape. The only reason why a customized sensor was not designed and ordered from Tekscan for this study, is that they prescribe a minimum order amount of these sensors which would have made it very expensive. Figure 25 shows an example of a custom sensor.

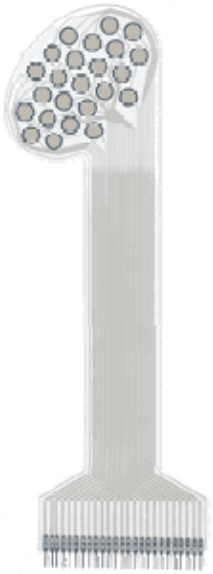

Figure 25: Example of custom sensor [49]

One of the main difficulties encountered while working with the single FSRs was that the lead wires tend to break easily where they are attached to the FSRs. Each FSR has two metal plates at the bottom where a connection can be made, however these metal plates tore out of the polymer too easily when connected to wires. The use of a custom sensor can aid in this problem as it can eliminate the wires altogether designing the sensor so that the ends connect directly to the data acquisition box.

6.3.2 Inflatable bladder

As was mentioned earlier, the inflatable bladder was a component in a wrist blood pressure monitor that was bought for the specific goal of using the bladder. Initially a normal hand pump and arm blood pressure monitor was purchased to perform initial testing of the concept. This blood pressure monitor had a large strap that goes around the upper arm and fastens with two Velcro strips. In the inside of this strap was a large rubber bladder with two tubes coming out. The one tube was connected to a hand pump and the second to a mercury pressure indicator.

For initial testing, the FSRs were attached to the surface of the strap using Scotch tape. Folding a towel around a pipe numerous times created a nice round and soft test rig. Small and large stones were inserted between different levels that were created by the towel. This portrayed the neck with different sized lymph nodes at different depths. The strap was then fastened around the towel with the FSRs positioned over the stone. The cuff was inflated to a certain pressure and the measurements were taken. This proved to be a successful test and further development of the concept followed. The rubber bladder though was to big to fit nicely into the neck brace. It was then decided to look for an alternative.

The alternative came in the form of a wrist blood pressure monitor purchased via the internet. Because this blood pressure monitor goes around the wrist, it is a lot smaller and the subsequent inflatable rubber bladder is also smaller. The monitor came complete with an air pump, valve, connectors and the inflatable bladder. It turned out that the bladder was exactly the right size and fits perfectly into the neck brace. The size of the bladder is 130 mm x 65 mm. The pressure is supplied to the back of the bladder with the special T-piece that was mentioned in the system layout section.

6.3.3 Pump, valve and control circuit

The pump and the valve was part of the blood pressure monitor that was purchased. The pump is a Koge Electronics pump KPM12A. The data sheet for the pump is attached as Appendix D. The valve is a spring loaded valve that is normally open. As soon as 3V or more is applied to the valve it closes.

Controlling the pump was one of the more difficult tasks of this study. It is necessary to control the pressure in the system rather accurately with the pump. The pump is controlled using a computer's sound card as an analogue output port. Python is the programming language used in the study. Using the Python Tkinter module it is possible to set up the sound card according to the user's requirements and produce an output. The volume setting will determine the magnitude of this output. The program will be discussed in Section 6.4.

The only disadvantage of using the sound card is that the sound card output could only produce an alternating or periodic signal with a peak voltage of 0.6 V. The pump requires 3 V DC power. Amplifying the signal with a basic inverting amplifier circuit and eliminating the negative portions of the signal with a bridge rectifier produces a larger, positive signal. The signal is then smoothed out using a capacitor in order to resemble a DC signal. The sinusoidal signal is amplified to 3V, it is rectified using the bridge rectifier and the ripples were reduced

by simply inserting a capacitor. This all worked excellently when checking the signal using an oscilloscope. The current supplied by the sound card though was too small to switch on and control the pump. Two solutions were investigated, a current amplifier circuit and using a relay to simply switch the pump on and off. The advantage of the current amplifier circuit is that it is still possible to supply the pump with a varying voltage, i.e. operating the pump at different power as the situation demands.

The current amplifier circuit that was investigated uses a Bipolar Junction Transistor (BJT) connected as a common collector. This circuit is known as an emitter follower and is shown in Figure 26. This circuit was connected between the pump and bride rectifier. Even though it switched on the pump, it took the pump about three minutes to inflate the bladder to the necessary pressure. This is due to the small amplifying constant given by the circuit.

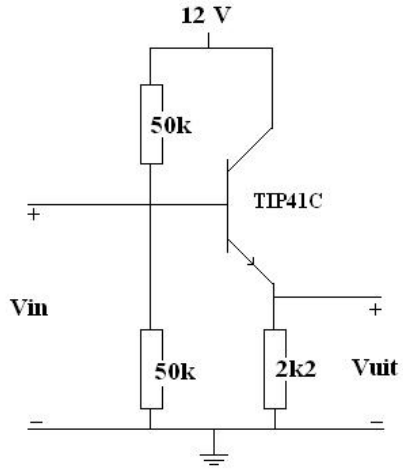

Figure 26: Emitter follower

The second solution was to use a relay. A 5 V relay was used to switch the current supplied by one of the 9 V batteries to and from the pump. Using this method the pump was simply switched on at a certain power and switched of again when the pressure was reached. Using PID control was no longer possible. The pump is simply switched on for a certain length of time which will allow the pressure to reach the necessary value. Figure 27 shows a schematic of the final control circuit.

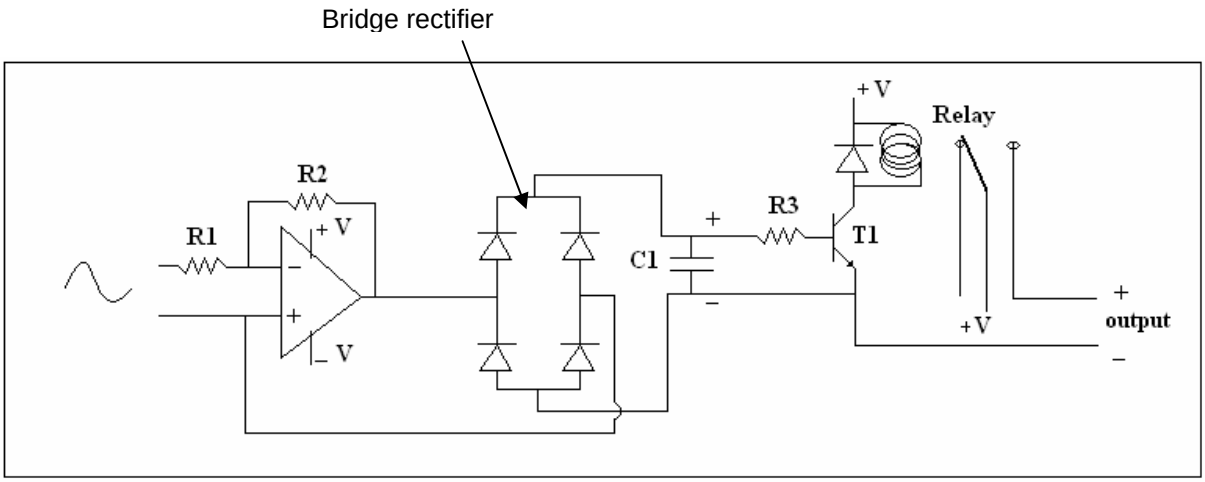

Figure 27: Pressure control circuit

The combination of R1 and R2 was chosen to give an amplification of around seven. This is to ensure the peak voltage of the sinusoidal signal is greater than 3 V. R3 was chosen to saturate the transistor at the required collector current as required by the relay resistance. Table 4 indicates the main components.

Table 4: Main components of pressure control circuit

R1	4.7 kΩ
R2	33 kΩ
R3	47 kΩ
C1	100 nF
T1	2n222
Relay	5 V DC

Other methods of controlling the pump that was investigated include a PIC microcontroller and a PLC. The disadvantage of using a PIC microcontroller is that the required pressure is a constant that gets loaded onto the microcontroller and thus is difficult to change.

A PLC can provide an easy to use interface as well as PID control for the system. Disadvantages of using a PLC include costs of a PLC and the fact that different software is used to control the PLC than what is used for the image registration algorithm. Using Python to control both the pump, image registration and set up a user interface is the one big advantage of using the sound card. There are also no extra costs as Python is a freeware software language.

6.3.4 Pressure Sensor

The pressure sensor used is a FESTO SDE1-D2-G2-WQ4-C-PU-M8. It has two air inputs and a four pin electronic connection. The electronic connection provides the required 24 V operating power as well as the analogue output. The operating pressure of the sensor is 0-2 bar and the corresponding analog output is 0-10 V with an accuracy of 3% at a temperature of 20-25 °C. The sensor also has a large display showing the current pressure sensed.

The sensor can be used to provide an analogue output of 0-10 V corresponding to a pressure of 0-2 bar, or the sensor can be used to set certain set points. Two pressure values can be set as set points and as soon as that point is reached, a digital signal is sent.

The sensor was originally purchased for its analogue output ability. This was meant to be used as a feedback control to the control circuit. Due to the fact that the control circuit uses a relay it is no longer necessary to use the analogue output capabilities of the sensor. The sensor was used to set up the correct times needed to inflate the bladder to the required pressure. The sensor now merely serves as a pressure indicator. Figure 28 shows a picture of the sensor. The data sheet of the sensor is attached in Appendix E.

Figure 28: Pressure sensor

6.3.5 Data acquisition box

Designing and constructing the data acquisition box required the help and expertise of two German exchange students, Sven Queisser and Alexander Bögel.

The functional requirements of the data acquisition box was that it should be able to convert the change in resistance of a FSR into a digital value that can be used to represent the force experienced by the sensor. A further requirement was for the data acquisition box to have numerous input ports for the sensors.

An easy way to represent a variable resistance (as in the case of the FSRs) as a voltage is to use a voltage divider circuit. Figure 29 shows a schematic of a voltage divider circuit.

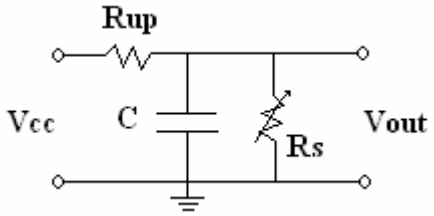

Figure 29: Voltage divider

The relationship between the measured voltage and resistance is:

$$V_{OUT} = \frac{R_S}{R_S + R_{UP}} V_{CC} \tag{12}$$

- Where R_S is the variable resistance (FSR)
- R_{UP} is the pull-up resistor and is 47 kΩ
- V_{CC} is the reference voltage and in this case it is chosen to be 5 V
- V_{OUT} is the measured voltage, and
- C is a capacitor chosen to act as a low pass filter. C = 100nF

In order to eliminate high frequency distortion and noise it was decided to use a low pass RC network. This is achieved by simply adding the capacitor as shown in Figure 29. The edge frequency for this circuit now becomes:

$$f_C = \frac{R_{UP} + R_S}{2\pi R_{UP} R_S C} \tag{13}$$

With no sensor connected, f_C = 34 Hz. Connecting a sensor and decreasing the resistance will cause f_C to increase. The sampling rate must always be lower than f_C to eliminate high frequency noise and not the measured signal. The signals will change very slowly and thus a sampling rate of 1 Hz is sufficient which will always be below f_C.

Now that the sensor circuit is designed the next step is to convert these signals into digital signals. This is done using an Atmega8 microcontroller from Amtel and six 8 to 1 multiplexers. These six multiplexers will enable 48 sensors to be connected and measured. Figure 30 shows a schematic of the microcontroller with the six multiplexers.

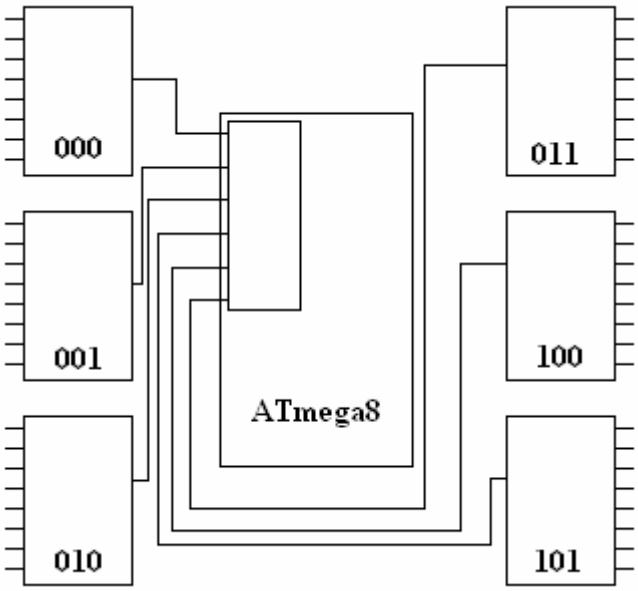

Figure 30: Microcontroller with multiplexers

The outputs of the six multiplexers are each connected to an A/D input terminal on the microcontroller. These six A/D channels of the microcontroller are the inputs to an internal multiplexer. Both the internal multiplexer and external multiplexers require a 3-bit address to select the appropriate input. The 3-bit address of each multiplexer is shown in Figure 30. To select between the eight input signals (which will be the output voltage from the voltage divider circuit) each multiplexer can choose between address 000 and 111.

The three address bits of the external multiplexers (lower bits) and the three bits of the internal multiplexer forms six bits of the eight bit input address. This is illustrated in Figure 31

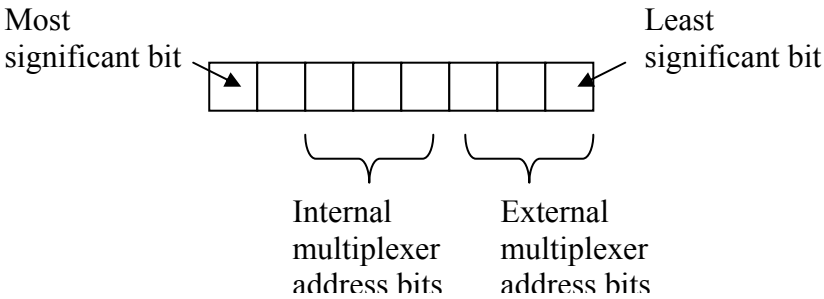

Figure 31: 8-bit address

With these six bits, any of the 48 sensor values can be converted to a digital value. The microcontroller converts the analog signal into a 10-bit digital value, or a value between 0-1023.

The next step is to send these values to a computer. It was decided to communicate using the computer's RS232 port. This was chosen because it is an easy and simple way of communication which will decrease programming time. To create a standard RS232 interface a level converter is required to convert the TTL-compatible levels of the microcontroller to ±12 V levels for the interface. The MAX232 from Maxim was used as the level converter.

The RS232 port is a serial communication port. That means that the data is sent and received bit by bit. The communication protocol is a line-orientated text based protocol. This can be used with any terminal-emulator or any custom higher level software. This makes the initial testing of the data acquisition easier using Windows' Hyper Terminal. In later stages of the thesis project Python can be used as communication software.

Each time a key is pressed there is an interrupt which is handled by the UART. When such an interrupt occurs, a character is received and placed in a buffer. Characters are received until a line feed arrives or an overflow occurs. After a whole line is received, a receive interrupt flag is set to notify the main program. The main program will then check whether it recognizes the line or not. There are a couple of commands that the program will check for. These commands and a description of the program are attached in Appendix F.

6.3.6 Neck brace

The neck brace provides the main structure for the entire system. This is the part that is in contact with the patient and all the necessary parts should by mounted on or in the neck brace. The neck brace was purchased at a biomedical conference in Germany specifically to use for the project.

As described earlier, the neck brace is divided into four parts, top left, top right, bottom left and bottom right. Between the upper and lower parts on either side are inflatable rubber bladders. These rubber bladders enable the neck brace to stretch in length on either side and it is controlled using two hand pumps. This neck brace is actually used for patients with neck and spinal problems. This unique feature however enables the inflatable bladder with the sensors attached to move against the patient's neck.

6.4 COMPUTER CODE

This section will discuss the Python code used to control the entire procedure from inflating the bladder to the image registration algorithm. This section will be divided into four sections:

1. Structure
2. Sound card
3. Reading data
4. Final Image

6.4.1 Structure

The structure or user interface is an important part of any program or software. This ensures ease of use and serves as a means to display the necessary information. The structure in its raw state is just an empty frame called the parent frame. Here numerous sub-frames are allocated to certain positions on the parent frame. Each part of the user interface exists in its own frame and include:

- Information frame
- Images frames

- Pressure frame
- Final image frame
- Notes frame
- Help frame

These can be seen in Figure 17. Each frame defines its individual buttons, labels or graphics that it should display. The buttons are linked to certain commands it carries out when clicked.

At the top of the parent frame is a menu bar. The menu bar has two buttons which opens drop down menus, these are the file button and help button. The file drop down menu include new, save and exit options. The help button provides the user with a guideline which appears in the Help frame.

6.4.2 Sound card

The computer's sound card is used as an analogue output. This is used to send a sinusoidal signal to the pressure control circuit. In order to set up the sound card and control the output using Python, the tkSnack module is required. This can be downloaded as freeware from the internet.

Two functions are defined which are used to set the volume and to play a note. Playing a note requires the use of a filter. The tkSnack module provides the filter and it is only necessary to specify the frequency, duration and type of signal. A frequency of 600 Hz is used with a sinusoidal signal. The duration depends on the pressure required.

6.4.3 Reading data

Reading the data produced by the sensors requires a Python Module enabling communication with the RS232. The PySerial module was used for this purpose. All the necessary parameters are set as listed in Table F-1 in Appendix F. The serial port is then opened and the command "READ ALL\n" is given. The "\n" command signifies a line feed. Once this command is given a list indicating all the sensor values is returned to Python. The value of each sensor is first converted to a force with a revised equation of that suggested by Berger and Hess [31]:

$$F = 3.2232 \times 10^{5} \times x^{-2.4095} \tag{14}$$

Equation (14) is modified from an eight bit to a ten bit equation. This means that the measured value is in the range 0 – 1024 instead of 0 – 254.

A vector is created and the force value of each sensor is placed in its corresponding position in the vector. This vector is then changed into a 5x5 matrix. This step is repeated for each of the 25 required images. The images are displayed on the user interface.

6.4.4 Final Image

Once all the images are read and available, the final image can be formulated. The final image is a combined image of all the other images. To get a smoother end product all the images taken are scaled to a 17x17 matrix as an initial step before super resolution. This is done by simple linear interpolation. The 3x3 matrix in Figure 32 helps to illustrate this.

a1	b1	a2
b2	b3	b4
a3	b5	a4

Figure 32: Linear interpolation

Suppose the grey blocks in Figure 32 are the original elements in a 2x2 matrix. To scale the matrix once will require five new elements to be added as shown by the white blocks in Figure 32. The values of the newly added white blocks are simply the average of their neighboring grey elements. Thus the value for b1 will be (a1+a2)/2 and b2 is (a1+a3)/2. The value of b3 now becomes (a1+a2+a3+a4)/4.

After the matrices are scaled they are normalized by dividing each element by the largest element in the respective matrix. This ensures that the largest element in each matrix has a value of one. Image registration can now begin.

X1 or the first matrix serves as the reference matrix. The second matrix, X2, is now transformed. This is done by first determining the new x and y values corresponding to the different elements in the matrix. If the image has to move to the left by one pixel for instance, the original position at (0,0) now becomes (0,1) thus the new x value is 1. If the image moves to the left and up the coordinates of position (0,0) becomes (1,1). This is illustrated in Figure

33. The positions now occupied by blank spaces receive a constant value of 0.23920232. This is the average value of a sensor when it presses against soft tissue.

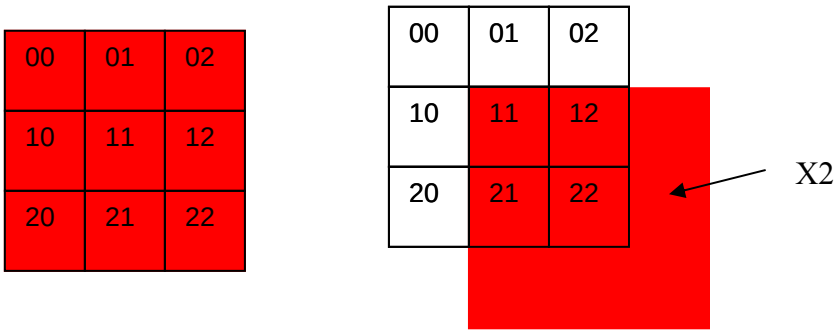

Figure 33: Transformation of X2

Determining the new x and y values is done using the Fourier-Mellin transform:

$$\begin{aligned} x_{NEW} &= x\cos\theta - y\sin\theta + tx \\ y_{NEW} &= -x\sin\theta + y\cos\theta + ty \end{aligned} \tag{15}$$

The variables *tx, ty* and θ are the variables that must be solved for using an optimization technique to get X2 to be sufficiently transformed to fit nicely onto X1. A measure of goodness of fit is to subtract the two matrices from each other, take the square of each element and then sum the remaining element values together as described by equations 3 and 4.

$$\chi^2(a) = \left\| X_1(x) - X_2(f(u)) \right\|^2$$

and in discrete form this becomes

$$\chi^2(a) = \sum_{i=1}^{N} \left[X_1(x_i) - X_2(f(u_i)) \right]^2$$

If the two matrices are an exact fit, the answer will be zero. Thus the minimum value will be the optimum fit.

Using the built-in optimization technique fmin_powell, Python adjusts the values for *tx, ty* and θ in an effort to find the minimum value for χ^2. The values for x_{NEW} and y_{NEW} must be integers because referencing a position in a matrix requires two integers (the *x* and *y* positions). These x_{NEW} and y_{NEW} values must therefore first be rounded before the new X2 is calculated. The transformed X2 is constructed using the values of the old X2 corresponding to

the positions of x_{NEW} and y_{NEW}. Once X2 is sufficiently transformed, the average between X1 and X2 is taken and set as the new reference X1.

$$X_1 = \frac{X_1 + X_2}{2} \tag{16}$$

The whole process is then repeated using X3 and the new reference X1. After they are matched the result is a new reference X1 for the next matrix to be matched with. This process repeats itself for all 25 images.

After all the images are transformed and matched with the reference image this final reference image then becomes the final transformed image which is displayed. An indication of the size of the lymph node is calculated by counting the number of elements with a value higher than a specified value (this specified value is 0.8 at the moment). This gives an indication of the number of sensors that measured a harder surface which in turn gives an indication of the size of the hard object and it is displayed above the final image.

The hardness is determined as the highest value measured at a sensor in any of the images before they are normalized. This value is also displayed above the final image.

With the prototype built and the code working the testing could begin, but a model was required for testing.

7. TEST MODEL

In order to perform the different tests on the prototype a test rig has to be built. This test rig must accurately represent a human neck with numerous different sized lymph nodes present. This test model is supposed to have close to the same hardness of human tissue and underneath this soft tissue, a couple of hard, spherical objects.

After a lot of investigation into different products it was decided to use products by Smooth-on. Figure 34 shows an arm produced by the smooth-on products.

Figure 34: Smooth-on arm [50]

The arm is made using Alja-Safe™ alginate to form the mold and Ecoflex™ silicone rubber is cast into the mold to produce a soft arm. The Alja-Safe™ alginate is an alginate for life casting that does not contain crystalline silica which is a known cancer causing agent. It is an easy to use alginate which cures quickly and is ideal for making one-shot molds of any body part and it captures great detail.

The casting material is Ecoflex™ silicone rubber which is a softer than skin material and has a Shore A hardness of between 0 and 30. The silicone rubber cures quickly (within four hours) and it can be coloured with Silc Pig pigments. These two products were purchased from AMT Composites in Cape Town.

Making the silicone neck required the desired area to first be defined and this was outlined using tape. The Alja-Safe™ alginate was then applied to the area as shown in Figure 35. The Alja-Safe™ comes in a powder form and is mixed with water at a 1:1 ratio.

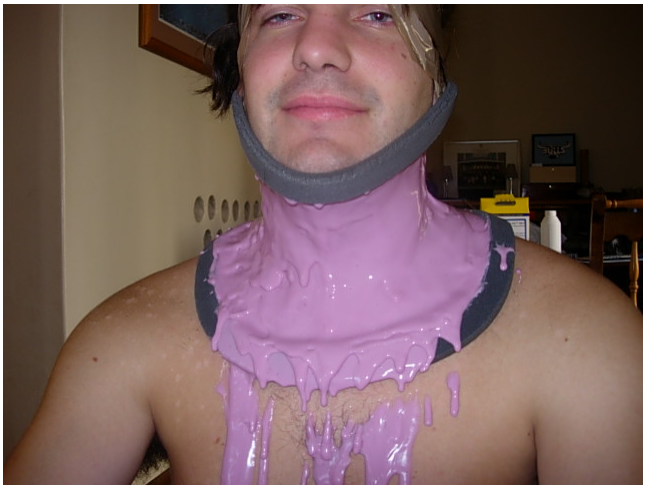

Figure 35: Applying alginate to desired area

As soon as the alginate dries it gets reinforced by a plaster layer to keep the alginate in its original form. This is shown in Figure 36.

Figure 36: Plaster reinforcement

Half an hour is given for the plaster to dry and harden before it is carefully removed. This is achieved by cutting the back end open and carefully removing the plaster. The alginate mold is also removed carefully by cutting it open as well but at a different spot. These are then left to dry while the silicone rubber is prepared.

The silicone rubber is prepared by mixing equal volumes of part A and part B of the Ecoflex™ together. A platinum catalyst is used to speed up the setting time of the silicone rubber. This is necessary because the setting time of the silicone rubber used is 4 hours but the alginate starts drying and shrinking after about 2 hours. This is due to the water that evaporates. Figure 37 shows the silicone being prepared. The two agents can be seen to the left.

Figure 37: Preparing the silicone rubber

The alginate mold with the now dry and hard plaster is positioned with a polystyrene core containing three different sized wooden beads. The beads are mounted on the core using wires and they are positioned in an area where lymph nodes will be present. The lymph nodes are two smaller ones and one large round one. One of the smaller nodes is round and the other one oval shaped. The silicone is poured into the mold and left to set. This is shown in Figure 38.

Figure 38: Adding silicone rubber to mold

The silicone is left to set for two hours. It is very important though to ensure that the bottom of the mold is thoroughly secured so that the silicone rubber does not leak out the bottom.

The model is soft when touched and feels similar to human tissue with the three lymph nodes detectable under the surface. It was later decided though to remove the larger lymph node and make an incision in the silicone neck 5 mm from the surface. This enables the use of different

shapes and sizes of objects to be inserted into the neck and sensed. The final neck is shown in Figure 39.

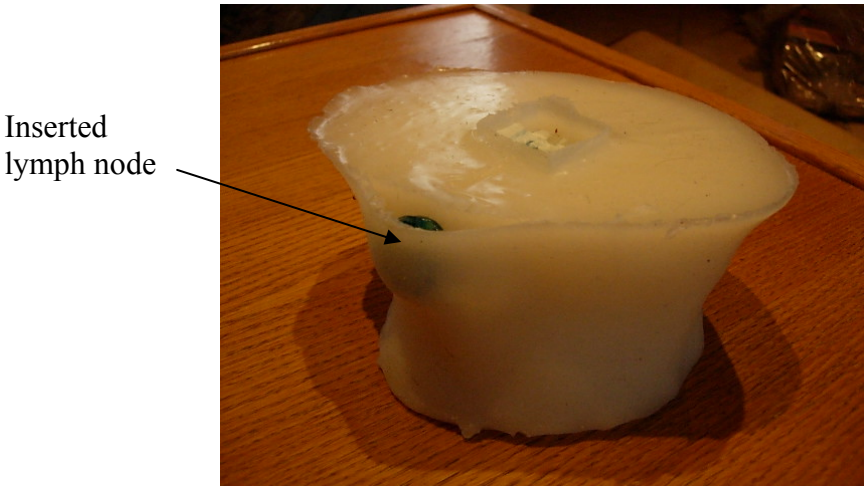

Figure 39: Final silicone neck

8. TESTING

In this section the different tests that were performed will be discussed. The section will be divided into five parts corresponding to the different tests that were performed.

1. Shape
2. Smallest object
3. Different sizes
4. Repeatability
5. Hardness

This section will describe the test procedure for each criterion. The results will be discussed in the next chapter.

8.1 SHAPE

The purpose of this test is to see whether the shape of a lymph node can be accurately sensed by the device. Different shaped objects were used and placed in the spot provided in the silicone neck. The prototype device was then used to make the necessary measurements. The final image of each shape is investigated to see whether the shape can be distinguished from it. This will be done for each of the shapes. The different shapes include a small sphere, a large sphere, a larger circular object and a rectangle. These are shown in Figure 40.

Figure 40: Different shaped objects

8.2 SMALLEST OBJECT

The purpose of this test will be to determine the size of the smallest object that can be sensed. This will be done by using objects smaller than and in the region of the size of a single FSR as the test objects. These include BB gun bullets and small beads which can be seen as the three objects in the left of Figure 41. The objects will each be placed in the spot provided and the testing will begin. The results of the test will give an indication of the smallest object that can be sensed.

8.3 DIFFERENT SIZES

Testing to see what effect different sizes have will be important. The device provides a number corresponding to the size of an object. This number is determined by counting the number of elements in the final image with a value higher than a defined limit. The purpose of this test will be to check the difference in size value for differently-sized objects. It will also become clear what percentage size increase is detectable. Spherical beads were used because of the wide variety of sizes and uniform shape that resembles a lymph node. These can be seen in Figure 41. Table 5 lists the diameter of each sphere.

Figure 41: Differently-sized beads

Table 5: Sphere sizes

Bead #	*Diameter [mm]*
1	4
2	7
3	10
4	12
5	15
6	20

8.4 REPEATABILITY

The results of this test will actually follow out of the other tests. This test will give an indication whether the same object produces similar results each time it is used as the test object. The shape test described in Section 8.1 will be repeated a number of times for each shape. The results of the test can be used to assess the repeatability. The produced shape in the final image as well as the size and hardness numbers will be used to make this assessment.

8.5 HARDNESS

Objects of different hardness will be used in this test. This will include the plastic beads as hard objects and a piece of silicone rubber as a soft object. The hardness number produced by the device will be used to assess the outcome of the tests.

These five tests will give an indication of how well the device meets the requirements of a neck palpation device. The next section will discuss the results of these tests.

9. RESULTS

The different tests as described in the previous section were performed using the device. The results will now be discussed for each test using the same structure as in the previous section.

9.1 SHAPE

The different shaped objects produced the results shown in Figure 42 to 45 respectively. It can be seen that the larger round object shown in Figure 42 does not really appear to be round in either the final image or the other images on the left hand side. This can be due to the flat surface of the object and the curvature of the brace. This curvature forces the bladder to take the same shape and the edges of the flat object is amplified. A sensor pressing against an edge will experience a greater pressure than one pressing against a flat or uniform surface.

The shape of the small spherical object in Figure 43 produces a more satisfactory result. The final image appears to be a small circular shaped object. This though can be the result of the fact that only one FSR sensed a hard object most of the time. The final image therefore looks like a smoother version of image 1 due to the scaling.

Figure 44 shows the results of the large spherical object. The result is a large circular shaped object with the maximum pressure experienced in the centre. This is what one would expect the result to look like. Some of the single images on the left hand side are poor representations of the actual object, but the final combined image is a better result. It can also clearly be seen that the object is larger than the small sphere in Figure 43.

The results of the rectangular object are shown in Figure 45. The final image shows something representing a rectangular object which is good. Looking at the images on the left it is clearly visible that two or three FSRs positioned next to each other were experiencing a harder object. This is exactly what was expected and the final image shows the combined image.

The results in this section indicate that the shape can be distinguished to some extent. The final images will never be exact representations of the sensed objects, but it will show a shape representing the object. Objects with complex shapes and edges are difficult to sense and

display correctly due to the poor resolution of the sensors as well as the way the sensors press against edges. The device works best with spherical objects with no edges. This is good because a lymph node is a spherical object.

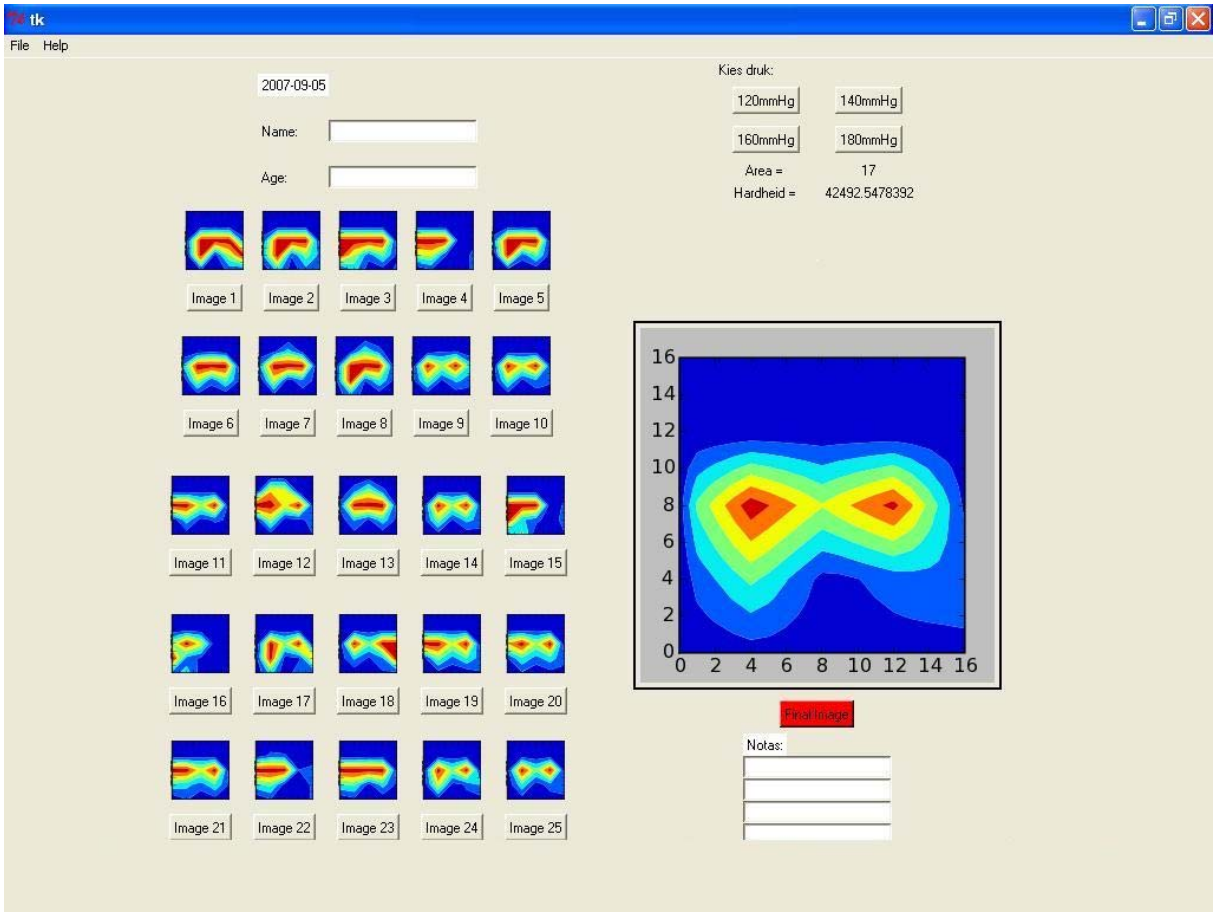

Figure 42: Result of large circular object

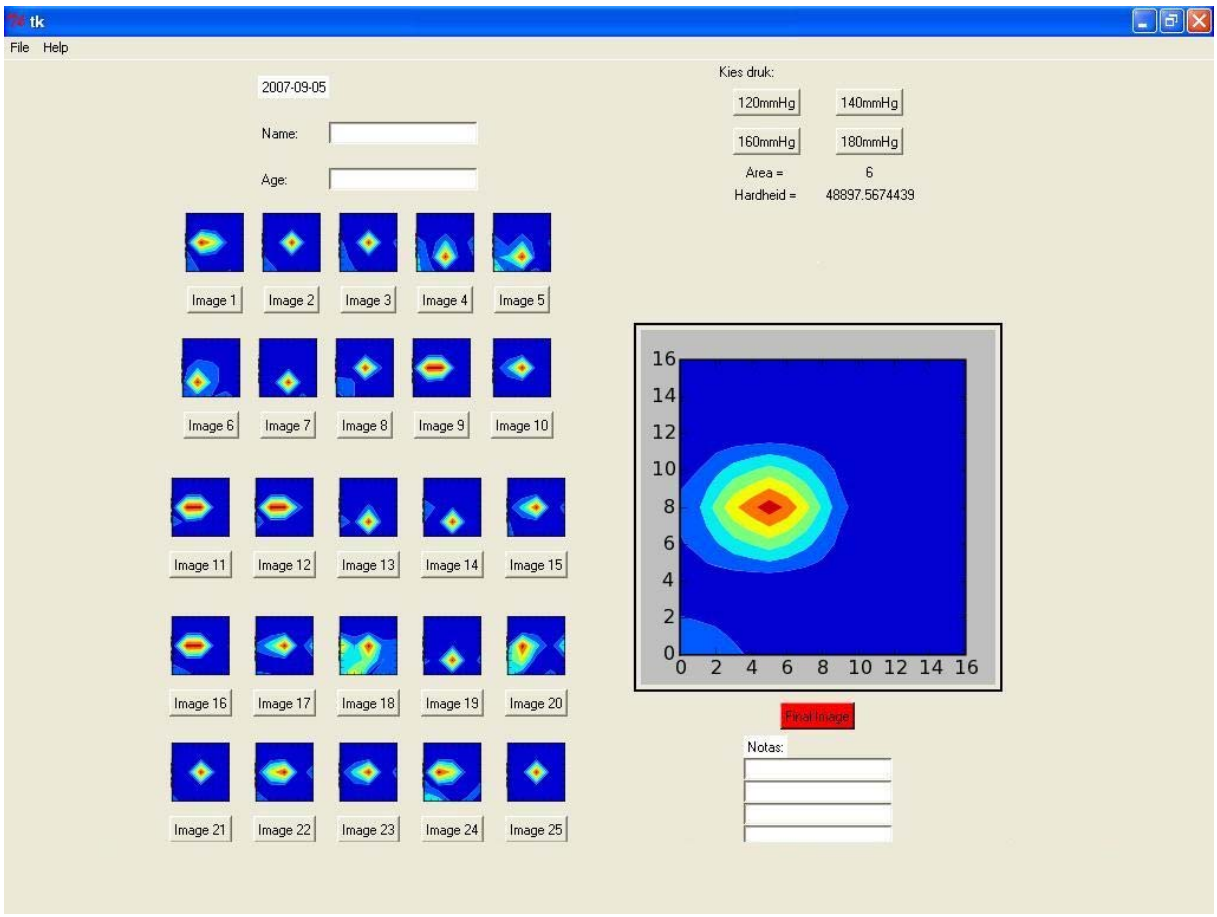

Figure 43: Result of small spherical object

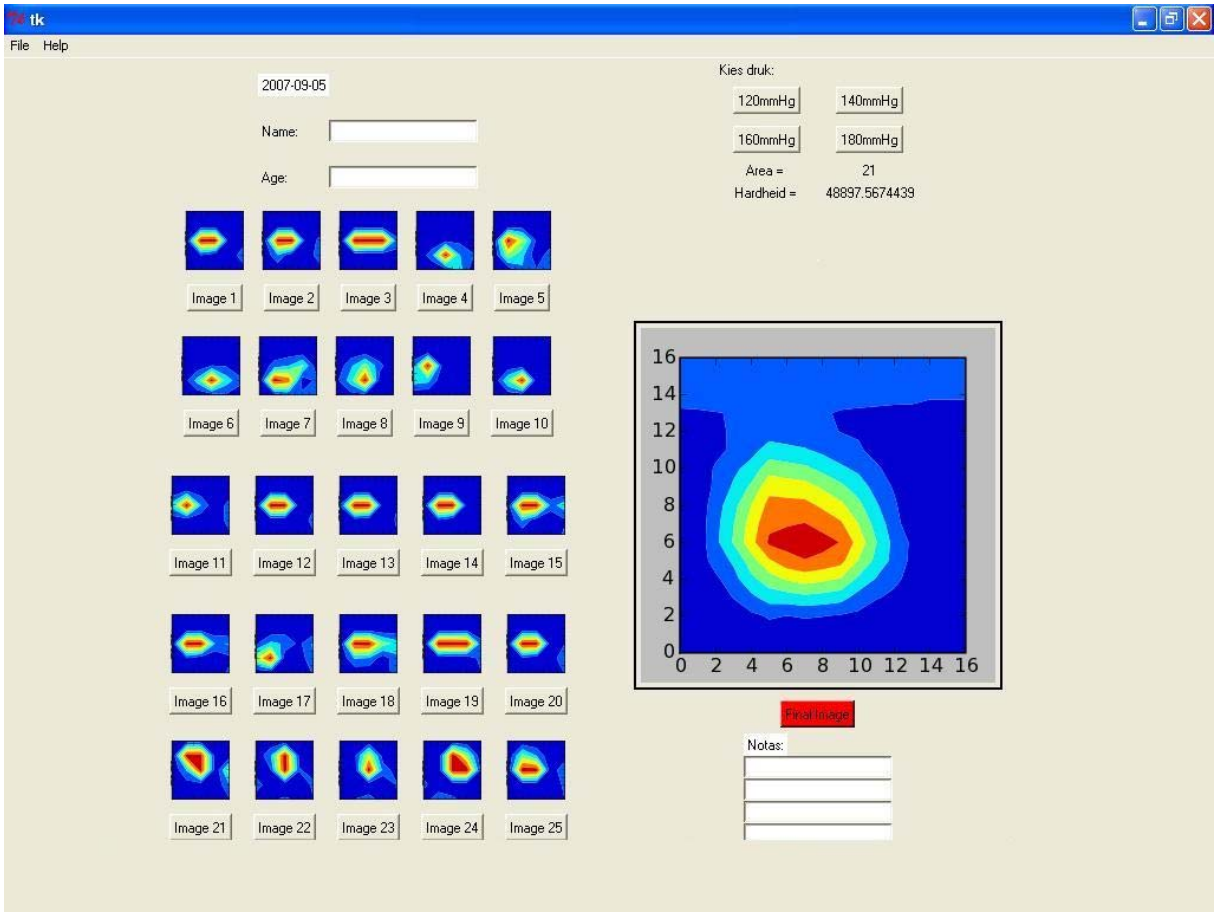

Figure 44: Large spherical object

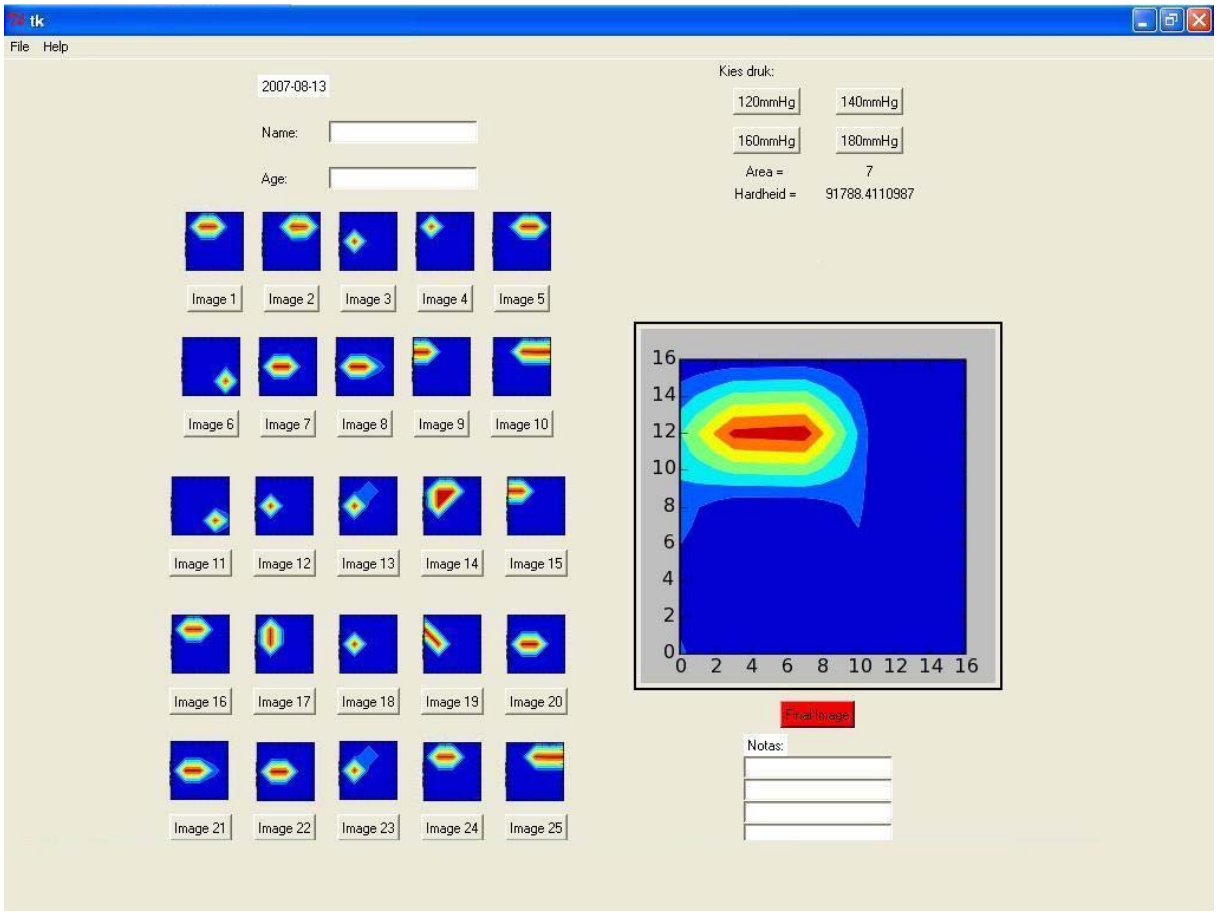

Figure 45: Rectangular object

9.2 SMALLEST OBJECT

The goal of this test was to see what the smallest object the device can detect is. The four smallest spheres were used. These have diameters of 4 mm, 7 mm and 10 mm respectively. The sensing area of each sensor is 8 mm. The smallest sphere, the 4 mm one, was not sensed at all by the device. This is due to the fact that the object is just too small. Once the object is placed into the neck it is impossible to tell where it is even using one's hands.

The 7 mm and 10 mm objects were measured without a problem. This is because they make a definite bulge when inserted into the neck. The results of these two tests are shown in Figure 46 and 47 respectively. The calculated number corresponding to the size of the objects were in the order of 5 to 7 for the two objects. This is taken as the smallest object that can be sensed. A healthy lymph node is in the range of 10 mm with an unhealthy lymph node larger than 15 mm in size. The size of an unhealthy lymph node will therefore definitely be detected.

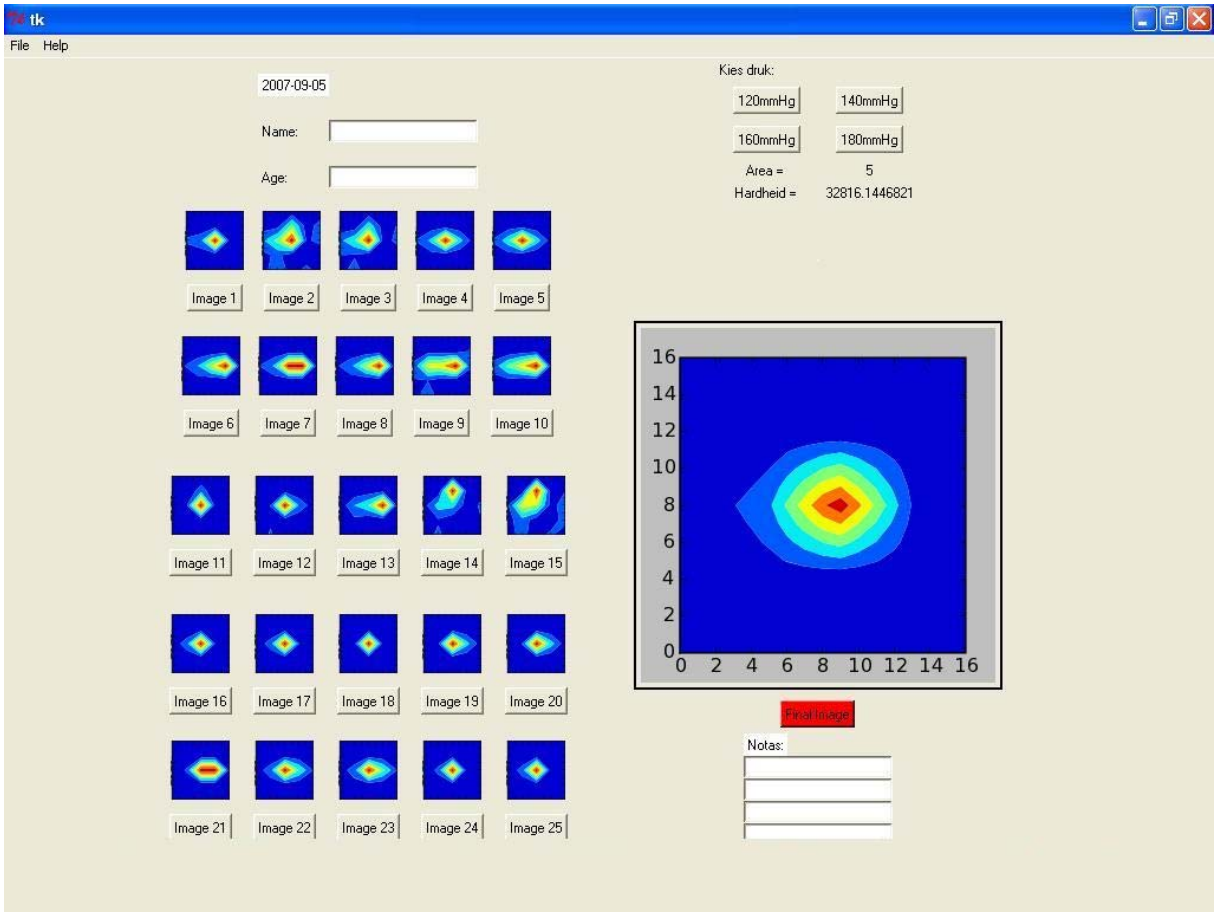

Figure 46: 7mm sphere

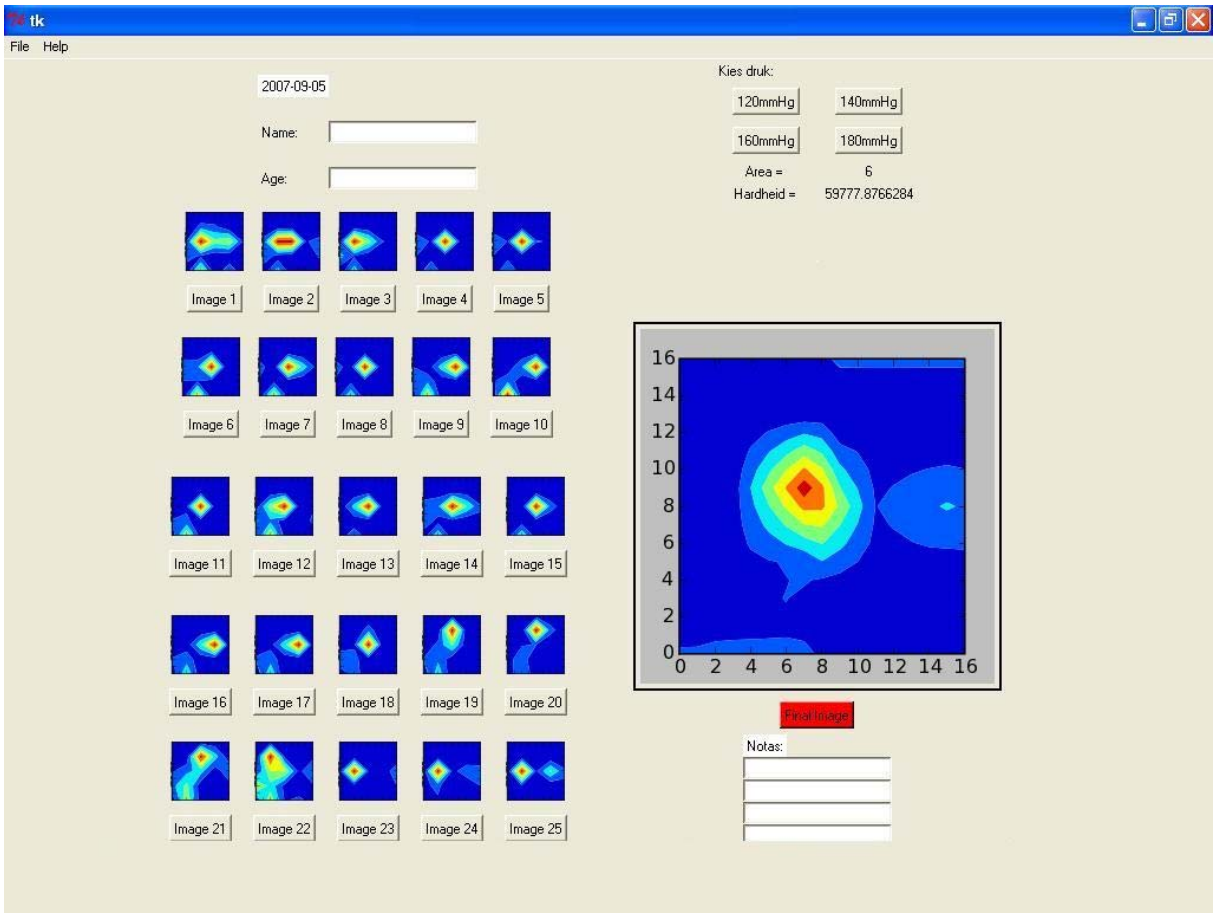

Figure 47: 10mm sphere

9.3 DIFFERENT SIZES

The tests performed here are meant to give an indication of the manner in which the device handles differently-sized objects. The emphases of the tests are on the calculated size numbers. This gives an indication of the relative sizes between the objects. The spheres as described in Section 8.3 were used. Table 6 gives a detailed list of all the tests showing the resulting image and the sizes and hardness values.

Table 6: Test results for different sizes

Results → / Bead ↓	1	2	3	4
1				
size	n/a	n/a	n/a	n/a
hardness	n/a	n/a	n/a	n/a
2	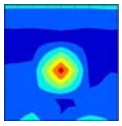	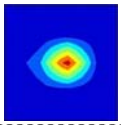	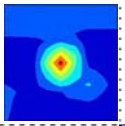	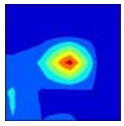
size	5	5	5	6
hardness	25047	32816	46619	23309
3	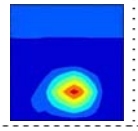	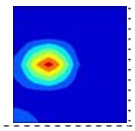	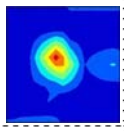	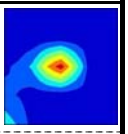
size	5	6	6	6
hardness	91788	48897	59777	119558
4	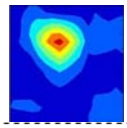	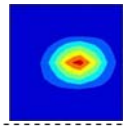	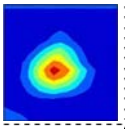	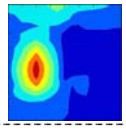
size	7	8	9	11
hardness	INF	86228	INF	64784
5	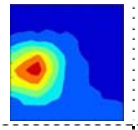	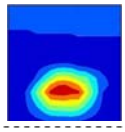	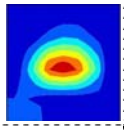	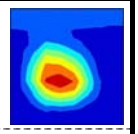
size	17	17	18	21
hardness	64748	83712	115484	48897
6	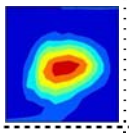	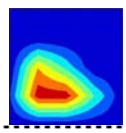	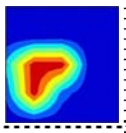	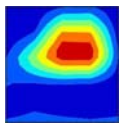
size	24	27	31	34
hardness	86288	88978	72335	91788

As was stated earlier, the smallest sphere could not be sensed and thus there are no results to display for it in Table 6. All the other results are shown. The difference in size can clearly be seen as the spheres increase in size.

The average sizes of spheres 2 to 4 do not change much although the difference is visible. The sizes for the larger three spheres differ all the time although a clear difference is evident between them. These changes in size can simply be accredited to the fact that the number of sensors detecting a hard object differ from time to time depending on the orientation of the object. This becomes more apparent for the larger sized spheres because they can cover two or three more sensors from time to time. The results are satisfactory as the difference in size can be seen and measured. Figure 48 plots the sphere sizes against the measured size for each.

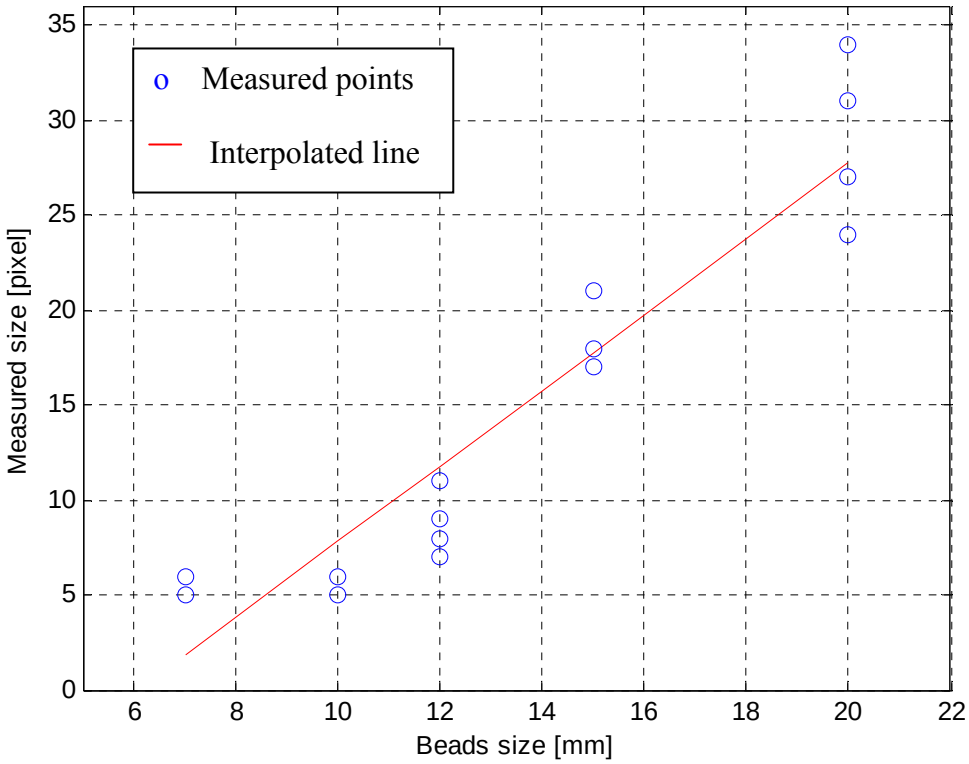

Figure 48: Sphere size versus measured size

9.4 REPEATABILITY

Looking at the images for each of the spheres in Table 6, it is evident that visually the images for each sphere look almost the same with respect to shape and size. The sizes for spheres 2 and 3 stay constant except for one small fluctuation. The sizes for spheres 4, 5 and 6 differ quite a lot. This could be because of the different number of sensors registering a hard object

each time. This will differ from image to image although the overall size should stay within a certain range for each size. There exist clear differences in size though for each of the spheres.

The one aspect that doesn't stay the same is the hardness. The hardness changes greatly for each sphere. For sphere 5 the value jumps from 48897 to 115484. This is an increase of more than 100%. The reason for such drastic differences is because the highest value of a sensor out of the 25 images is taken. This value depends on an individual sensors value which will differ from image to image. This was not a good method of representing the hardness. A better method is to use the average value of all 25 images as will be discussed in the next section.

It can be noted that the value of hardness also increases as the size of the sphere increases. This is because the pressure was kept the same for all tests and for a larger object the initial pressure is greater than for a small object.

The hardness value is hence not repeatable although it will show a difference between hard and soft as will be discussed in the next section.

9.5 HARDNESS

Table 6 showed that the hardness value differs greatly each time. It still shows whether an object is hard or soft. Figure 49 shows the result for a soft object. A silicone sphere with a radius of 20 mm was used.

Figure 49 shows that the soft object was not sensed accurately by the device. The result does not show a definite shape and all the images were random noise. This is because there is little difference between the measured values of the sensors. They all sense a soft object underneath. The size was measured as 6 although the object was as large as the largest hard sphere. The hardness was measured as 12523 which is a lot smaller than the smallest value measured for a hard object. Using all this knowledge, it is possible to distinguish between a hard object and a soft one.

A better method of calculating the hardness is to use an average value and not the highest sensor value. This will eliminate random high values. The highest value of each image is taken and the average value of the 25 images is then used to represent the hardness. Table 7 lists the results using this method for the 20 mm and 15 mm spheres as well as for the 20 mm silicone sphere.

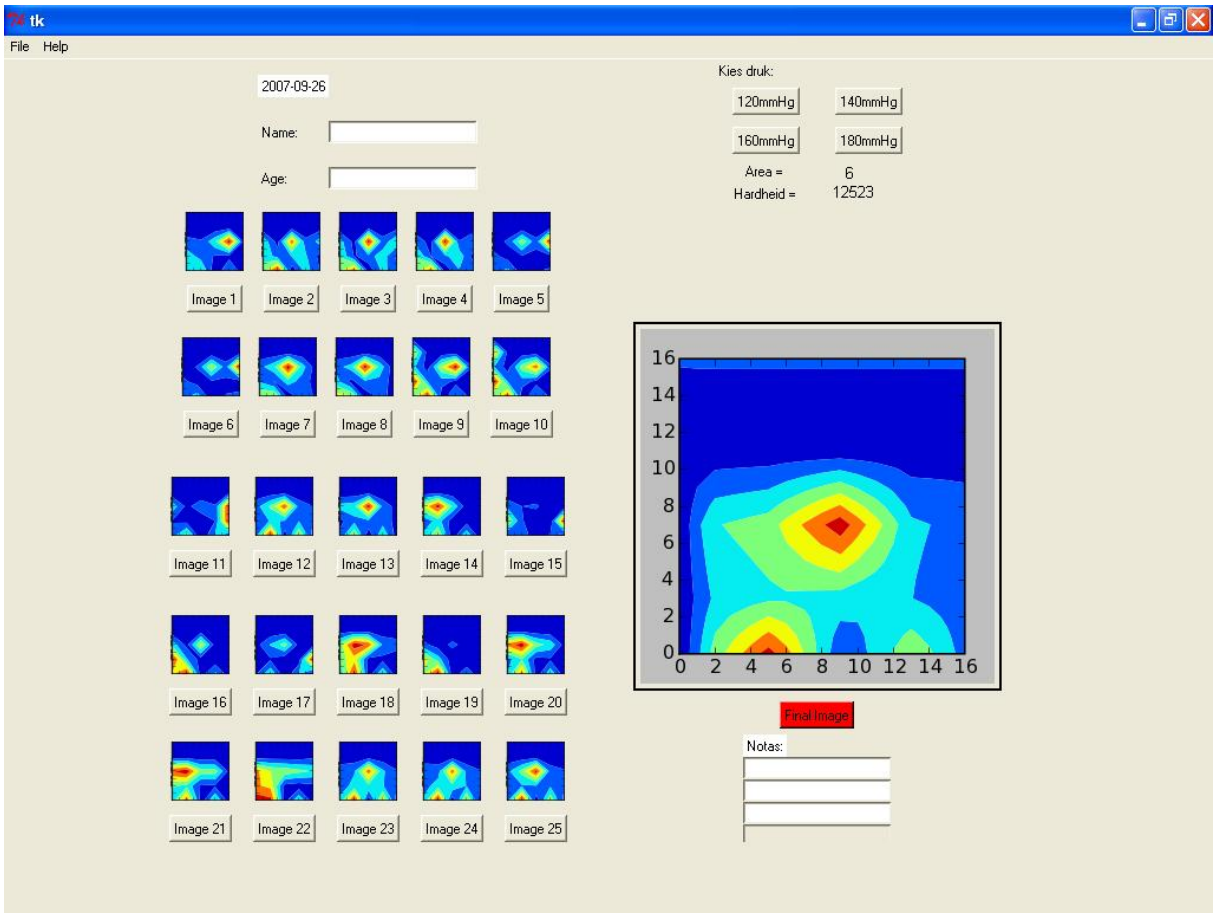

Figure 49: Result of soft object

Table 7: Hardness using average value

	Hardness number
20 mm hard sphere	20056
	30401
	25776
15 mm hard sphere	27270
	25516
	34353
20 mm soft sphere	6678
	9687
	10608

Table 7 shows that the variation in hardness number is greatly reduced although some variation is still present. This method has a variation in the order of 50 % compared to the variation of over 100 % for the previous method. The value for a soft object is also

significantly lower than for a harder object. The device will therefore be able to distinguish between a soft, small, healthy lymph node and a hard, swollen, unhealthy lymph node.

10. CONCLUSION

An abnormal sized mass in the neck is a common clinical finding and it can be the result of inflammation caused by bacterial or viral infection or it can be due to more serious diseases and malignant tumours. The most popular method of examining the neck is by manual palpation. Other methods include ultrasound, CT scan, MRI and PET. These methods though are expensive to perform and require specialists to interpret the results. The aim of this thesis was to design and develop a neck palpation device for telemedicine applications.

A lot of research has been done in the field of touch sensing and tactile sensing. These include sensors used for industrial applications as well as for biomedical applications. Many different touch sensors were investigated and compared to find the appropriate solution for the neck palpation device. FSRs are force sensors which has a change in resistance as a force is applied. This change has a logarithmic characteristic enabling the sensor to cover a large field. FSRs were used in the thesis because of their low cost, availability and robustness.

Two different concepts were developed and investigated with the inflatable bladder concepts proving to have the most potential. This is due to the fact that a uniform and repeatable pressure can be applied to the patient's neck each time. The concept consists of an array of FSRs attached to an inflatable rubber bladder. The bladder is inflated by a small air pressure pump which is controlled using a computer's sound card. A pressure relief valve is used to deflate the bladder. This is all mounted on a neck brace designed to fit comfortably around the patient's neck.

As the bladder is inflated, the FSRs press against he patient's neck and the measurements are taken. This step is repeated numerous times with the neck brace repositioned to gather more data. This data is used in an image registration algorithm to improve the resolution of the FSRs. The device was tested for shape, smallest size, different sizes, repeatability and hardness.

Complex shapes with numerous edges could not accurately be measured although basic shapes like different spheres and prisms could be distinguished between each other. The smallest size that was measured was a sphere with radius of 7 mm. The different sizes produced different results that can be distinguished. The smallest object yielded a size value of 5 while the largest object had an average size value of 29. All the differently sized objects

had different size numbers associated with them. In the size range of lymph nodes the different objects could be distinguished.

The repeatability of the shape and size were good but it lacked in the hardness tests. Although the values differed a lot it is still possible to distinguish between a soft and a hard object. The super resolution algorithm worked well and definitely contributed to the good results obtained for spherical objects such as lymph nodes.

The device performed all the tests satisfactorily and it showed that the device can be used to sense for hard spherical objects. The main shortcoming of the device is the low resolution of the images. The results though suggest that the main outcomes of the study were achieved. The device can be used in telemedicine environments for an initial check-up after which the results are sent to a doctor. The doctor will be able to see whether a hard lymph node is present and the size can be determined. The doctor can then advise the patient whether or not he should seek further tests.

Further work on the project can look at improving the resolution. This can be achieved by investigating different sensors. Sensors with a spatial resolution of smaller that 2 mm are suggested. The individual FSRs were also difficult to work with and a customized sensor would be ideal for the application. A customized sensor that is combined with the bladder will eliminate the use of an adhesive to attach the sensors. Clinical testing of the device is also necessary to see the effect of noise caused by different structures in a human neck.

REFERENCES

[1] Gosselin B.J., Neck, Cervical Metastases, Detection, Department of Surgery, Darmouth College, eMedicine Specialties [Online], [cited 2006, June 15], Available from: http://www.emedicine.com/ent/topic306.htm.

[2] SureTouch Visual Mapping System, [Online], [cited 2006, July 1], Available from: http://www.medicaltactile.com/suretouch.html.

[3] World Health Organization (WHO), The World Health Report 2000, Health Systems: Improving Performance, France, 2000.

[4] Martini F.H., Bartholomew E.F., Essentials of Anatomy & Physiology, 3rd edition, New Jersey, Prentice Hall, 2003.

[5] Armstrong W.B., Giglio M.F., Is this lump in the neck anything to worry about?, Postgraduate Medicine 2003; 104 (3): 1-4 .

[6] Kaufman C.S., Palpation Imaging: Current Status, University of Washington, White Paper, 2005.

[7] Enderle J., Blanchard S., Bronzino J., Introduction to Biomedical Engineering, 2nd edition, California, Elsevier Academic Press, 2005.

[8] Pruessmann K.P., Weiger M, Scheidegger M.B., Boesiger P. SENSE: sensititivy encoding for fast MRI, Magnetic Resonance in Medicine 1999; 42 (5) 952-962.

[9] Young H, Baum R, Cremerius U, *et al*., Measurement of clinical and subclinical tumour response using [18F]-fluorodeoxyglucose and positron emission tomography: review and 1999 EORTC recommendations, European Journal of Cancer 1999; 35 (13): 1773-1782.

[10] Rapacholi M.H., Essentials of Medical Ultrasound: A Practical Introduction to the Principles, Techniques and Biomedical Applications, 1st edition, New Jersey, Humana Press 1982.

[11] Crowder R.M., Tactile Sensing, Automation and Robotics, University of Southampton, [Online], 1998, [cited 2006, August 7], Available from: http://www.soton.ac.uk/~rmc1/robotics/artactile.htm.

[12] Dargahi J., Najarian S., Liu B., Sensitivity analysis of a novel tactile probe for measurement of softness with applications in biomedical robotics, Journal of Materials Processing Technology 2007, 183: 176-182.

[13] Fisch A., Mavroidis C., Melli-Huber J., Bar-Cohen Y., Haptic devices for virtual reality, telepresence, and human-assistive robotics, Biologically Inspired Intelligent Robots, Bellingham, SPIE Press, 2003.

[14] Dargahi J., Najarian S., Human tactile perception as a standard for artificial tactile sensing – a review, International Journal of Medicine and Robotic Computer Assisted Surgery 2004, 1: 23-35.

[15] Pierson J., The Art of Practical and Precise Strain-Based Measurement, 1st edition, Milford, 1999.

[16] Matsuzaki R., Todoroki A., Wireless flexible capacitive sensor based on ultra-flexible epoxy resin for strain measurement of automobile tires, Sensors and Actuators A: Physical 2007, 140 (1): 32-42.

[17] Amor A. B., Budde T., Gatzen H. H., A Magnoelastic microtransformer-based microstrain gauge, Sensors and Actuators A: Physical 2006, 129 (1-2): 41-44.

[18] DiLella D., Whitman L.J., Colton R.J., Kenny T.W., Kaiser W.J., Vote E.C., Podosek J.A., Miller L.M., A micromachined magnetic-field sensor based on an electron tunneling displacement transducer, Sensors and Actuators A: Physical 2000, 86 (1-2): 8-20.

[19] Trpkovski S., Wade S.A., Baxter G.W., Collins S.F., Dual temperature and strain sensor using a combined fiber Bragg grating and fluorescence intensity ratio technique in Er^{3+} -doped fiber, Review of Scientific Instruments 2003, 74 (5): 2880-2885.

[20] Stomeo T., Grande M., Qualtieri A., Passaseo A., Salhi A., De Vittorio M., Biallo D., D'orazio A., De Sario M., Marrocco V., Petruzzelli V., Prudenzano F., Fabrication of force

sensors based on two-dimensional photonic crystal technology, Microelectronic Engineering 2007, 84 (5-8): 1450-1453.

[21] Engel J, Chen J, Liu C, Development of a Multi-Modal, Flexible Tactile Sensing Skin Using Polymer Micromachining, TRANSDUCERS, Solid-State Sensors, Actuators and Microsystems, 12th International Conference on, 2003, 2 (8-12): 1027-1030.

[22] M.H. Lee, H.R. Nicholls, Tactile sensing for mechatronics: a state of the art survey, Mechatronics 1999, 9**:** 1-33.

[23] Stramm D., Designing a tactile sensor for medical examination at the human neck, University of Stellenbosch, Stellenbosch, June 2005.

[24] Stramm D., Designing a tactile sensor for medical examination at the human neck, University of Stellenbosch, Stellenbosch, July 2005.

[25] Kane B.J., A High Resolution Traction Stress Sensor Array for use in Robotic Tactile Determination, PhD Thesis, Stanford University, Stanford, 1999.

[26] Howe R.D., Cutkosky M.R., Sensing skin acceleration for slip and texture perception, Robotics and Automation, Robotics and Automation IEEE 1989, 1: 145-150.

[27] Basu P.R., Russel R.A., Trott G., Extracting 3-dimensional surface features from tactile data, Proceedings of the International Symposium and Exposition on Robots 1988: 908-920

[28] Buttazzo G., Dario P., Bajcsy R., Finger based explorations, Intelligent Robots and Computer Vision: Fifth in a Series 1986, 726 (1): 338.

[29] Fearing R.S., Binford T.O., Using a cylindrical tactile sensor for determining curvature, Robotics and Automation IEEE 1991, 7 (6): 765-771.

[30] Russel R.A., Parkinson S., Sensing surface shape by touch, Robotics and Automation, IEEE 1993, 1: 423-428.

[31] Berger A., Hess P., Designing a tactile sensor for medical examination at the human neck, University of Stellenbosch, Stellenbosch, 2005.

[32] Zokai S and Wolberg G, Image Registration Using Log-Polar Mappings for Recovery of Large-Scale Similarity and Projective Transformations, IEEE Transactions on Image Processing 2005, 14 (10): 1422-1434.

[33] Zitova B., Flusser J., Image Registration Methods: A Survey, Department of Image Processing, Academy of Sciences of the Czech Republic, Image and Vision Computing 2003, 21: 977-1000.

[34] Vandewalle P., Super-Resolution Imaging, IVRG – Images and Visual Representation Group, [Online], [cited 2007, June 22], Available from: http://ivrgwww.epfl.ch/research/topics/superresolution.html, June 2007.

[35] Brown L.G., A Survey of Image Registration Techniques, ACM Computing Surveys 1992, 24 (4): 325-376.

[36] Anandan P., A computational framework and an algorithm for the measurement of visual motion, International Journal of Computer Vision 1989, 2: 283-310.

[37] Szeliski R., Image mosaicing for tele-reality applications, Workshop on Applications of Computer Vision, IEEE 1994: 44-53.

[38] Wolberg G., Zokai S., Image registration for perspective deformation recovery, SPIE Conference on Automatic Target Recognition X 2000, 4050: 259-270.

[39] Schwartz E.L., Topographical mapping in primate visual cortex: History, anatomy and computation, Visual Science and Engineering, Models and Applications, New York, Marcel-Dekker, 1994.

[40] Schaffalitzky F., Zisserman A., Viewpoint Invariant Texture Matching and Wide Baseline Stereo, Computer Vision 2001, 2: 636-643.

[41] Tuytelaars T., and Gool L.V., Wide baseline stereo matching based on local affinely invariant regions, 11th British Machine Vision Conference, 2000.

[42] Lucchese L., Cortelazzo G.M., Monti C., High resolution estimations of planar rotations based on fourier transform and radial projections, ISCAS 1997, 2: 1181-1184.

[43] Castro E.D., Morandi C., Registration of translated and rotated images using finite fourier transforms, Pattern Analysis and Machine Intelligence 1987, 9 (5):700-703.

[44] Ullman D.G., The Mechanical Design Process, 3rd edition, New York, McGraw Hill, 2003.

[45] Kaufman C.S., Jacobson L., Bachman B.A., Kaufman L.B., Digital documentation of the physical examination: moving the clinical breast exam to the electronic medical record, The American Journal of Surgery 2006, 192: 444-449.

[46] Ables D.C., Son J.S., Kaufman C.S., Sarvazyan A.P., The science behind electronic palpation: quantifying the sense of touch used in the clinical breast exam, University of Washington, 2006.

[47] Ables D.C., Son J.S., Egorov V., Sarvazyan A.P., Development of a device for documenting the clinical breast exam using a capacitice tactile array sensor, Artann Laboratories, Los Angeles, 2007.

[48] Willis C., Android World, [Online], [cited 2007, July 4], Available from: http://www.androidworld.com/prod59.htm.

[49] Tekscan, FlexiForce ® OEM and Custom Force Sensing Designs, [Online], [cited 2007, August 20], Available from: http://www.tekscan.com/flexiforce/OEM.html.

[50] Smooth-on, Life Casting, [Online], [cited 2007, September 25], Available from: http://www.smooth-on.com/lifecasting.htm.

APPENDIX A: IMAGING MODALITIES

A-1 Ultrasound

Ultrasound is a procedure in which high-energy sound waves are bounced off internal tissues or organs and make echoes. The echo patterns are shown on a screen forming a picture of body tissue. Ultrasound scans are performed by medical health care professionals called sonographers. Sonographs of metastatic lymph node disease characteristically find enlargement with a spherical shape. According to Gosselin the borders of the image is poorly defined in certain cases and lymph nodes of border line size cannot be reliably diagnosed using ultrasound alone.

Ultrasound is generally regarded as a safe means of testing because it does not use ionizing radiation which can cause cancer and breakdown of chromosomes. However, according to Rapacholi ultrasound energy has two physiological effects. It enhances inflammatory response and it can heat soft tissue. When ultrasound enters the body, it causes molecular friction and heats the tissue slightly. In some cases it can also cause cavitation, small pockets of gas in body fluids or tissue. The long term effects of tissue heating and cavitation are not known.

A-2 CT scan

Computed Tomography (CT) is a medical imaging method employing tomography (imaging by sections) where digital geometry processing is used to generate a three-dimensional image of the internals of an object. This is achieved by using a large number of two-dimensional x-ray images taken at each section around a single axis of rotation. Modern scanners allow the data to be reformatted in various planes or even as a volumetric representation of structures.

Since the birth of CT scans in the 1970s, it has been an invaluable tool in all fields of medicine, including the evaluation of neck cancer. The ability of CT to represent the data in various planes is an obvious advantage for assessing tumour spread in arbitrary oblique planes.

Figure A-1: CT apparatus in a hospital, Wikipedia

Figure A-1 shows typical CT apparatus in a hospital. Because it is a big and complicated machine, the cost to operate it is high. This is an obvious disadvantage to use it for a normal check up. Another disadvantage is that CT is regarded as a moderate to high radiation diagnostic technique. Too much exposure to radiation can cause radiation poisoning which is a form of damage to organ tissue.

CT scans rely on intravenously administered contrast agents to provide superior image quality which has a non-negligible risk associated with it. Certain patients may experience allergic reactions to these agents. The contrast agent may also induce kidney damage.

A-3 Magnetic resonance imaging

Magnetic resonance imaging (MRI) is a non-invasive method used to render internal images of an object. In contrast to CT scanning, MRI uses non-ionizing radio frequency signals to acquire its images and is better suited for soft tissue.

Medical MRI relies on the relaxation properties of excited hydrogen nuclei in plasma and lipids. When hydrogen atoms, which are present in all body tissues, are placed in a uniform magnetic field, their spins have to align in a particular manner with the applied magnetic field according to quantum mechanics. Spin refers to the angular momentum intrinsic to a body, and on quantum scale spin cannot be associated with rotation but instead refers to the presence of angular momentum. Hydrogen atoms have a spin of ½ and therefore they either align parallel or antiparallel to the magnetic field. The spin polarization determines the basic MRI signal strength

In order to selectively image different voxels (3D pixels) of an object, orthogonal magnetic gradients are applied. These gradients can be applied in any direction which enables MRI completely flexible orientations for images. This also gives MRI the advantage to assess tumour spreads in arbitrary oblique planes. Typical medical resolution is about 1 mm^3.

Figure A-2: Typical MRI apparatus in a hospital, Wikipedia

According to Pruesmann *et al* the MRI scanners used in hospitals cost approximately US$ 1 million per tesla (T) and have a typical field strength of 0.3 to 3 T, with several hundred thousand dollars paid per year for maintenance.

A-4 Positron emission tomography imaging

Positron emission tomography (PET) makes use of a short-lived radioactive tracer isotope, which is injected into the living subject (like the lymphatic system). This tracer isotope has been chemically incorporated into a metabolically active molecule and it decays by emitting a positron. There is a waiting period while the metabolically active molecule becomes concentrated in the tissues of interest after which the patient is placed in the scanner. The molecule most commonly used as the tracer isotope is fluorodeoxyglucose (FDG) for which the waiting period is approximately an hour.

As the isotope undergoes positron emission decay, it emits a positron which annihilates with an electron after traveling a few millimeters. This then forms a pair of annihilation (gamma) photons moving in opposite directions. Photomultiplier tubes or silicon avalanche

photodiodes detects these photon pairs when they reach a scintillate material in the scanning device which produces a burst of light. PET imaging produces a three-dimensional image or map of functional processes in the body.

PET has been extensively studied in the staging of head and neck cancer. The technique relies on the isotope FDG in metabolically-active lesions. Combining PET with CT scan can help to facilitate the location of the lesion of concern. In comparing the usefulness in the detection of cervical metastasis, PET/CT fusion images have been found to be superior and more accurate for the detection of cervical metastasis, compared to PET alone, as well as conventional imaging modalities. In addition, PET can contribute to the detection of residual or early recurrent tumours, leading to the institution of earlier salvage therapy.

Limitations to the widespread use of PET arise from the high cost cyclotrons needed to produce the short-lived radioactive isotope and the need for specially adapted onsite chemical synthesis apparatus to produce the radiopharmaceuticals. Although PET is non-invasive, it does involve exposure to ionizing radiation. Figure A-3 shows a typical PET facility.

Figure A-3: Typical positron emission tomography facility, Wikipedia

APPENDIX B: TACTILE SENSING

B-1 Mechanically based sensors

A mechanically based sensor is the simplest form of touch sensor. The applied force is used to activate a conventional mechanical micro-switch to form a binary touch sensor. The force required to operate the switch can be controlled using a spring with specific stiffness. The shortcomings of such a sensor are apparent as it only gives you information of whether the switch was activated or not. It gives no information on the magnitude of the applied force.

B-2 Resistive based sensors

Resistive based sensors are very common and widely used because of its simplicity and ease to manufacture. It is based on the use of a material with a defined force-resistance characteristic. The measurement of the resistance between two points on this material, usually a conductive elastomer or foam, gives an indication of the applied force. Figure B-1 depicts this behavior.

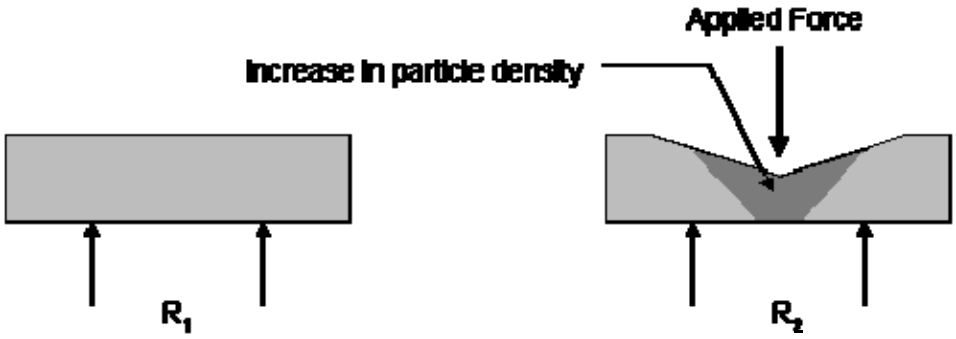

Figure B-1: Resistive based touch sensor, [11]

In Figure B-1 the applied force causes deformation of the elastomer which alters the particle density, resulting in the change in resistance. This simple design though does have disadvantages, including a non-linear time constant and a non-linear force-resistance characteristic of the elastomer, and the poor long term stability due to permanent deformation caused by cyclic loading.

B-3 Capacitive based sensors

A capacitive based sensor relies on the applied force changing the distance between two parallel plates or the effective surface area of the capacitor. This will cause the capacitance to change according to $C = \varepsilon A/d$, where A is the plate Area, d is the distance between the plates and ε is the permittivity of the dielectric medium. A problem with the capacitive based sensor is that the absolute capacitance decreases as the size of the sensor decreases to increase spatial resolution. Furthermore, problems can arise with sensors which is in close proximity to earthed metal structures or wires which leads to stray capacitance. This was a main factor why this method was not used for the neck palpation device as there would be a lot of wires running from each sensor to a data acquisition box.

It is possible to fabricate a parallel plate capacitor on a single silicon sheet which can give a very compact sensing device, but the process would have to make use of micromachining to manufacture this three-dimensional object. This is a complicated process.

B-4 Magnetic based sensor

There are two approaches in designing a touch sensor based on magnetic transduction. Firstly, a force applied to a magnet, causing it to move, will change the flux density at the measured point. This change in flux density can be measured with the Hall effect for which the Hall voltage is given by $V = -IB/dne$, where I is an applies current across the plate length, B is the magnetic flux density, d is the depth of the plate, e is the electron charge, and n is the bulk density the carrier electrons.

Secondly, the force can be applied to the core of the transformer which is manufactured from a magnetoelastic material. A magnetoelastic material is a material whose magnetic characteristics are modified when the material is subject to changes in externally applied forces. The magnetoelastic core will deform and cause the magnetic coupling between transformer windings, or a coil's inductance to change.

According to Crowder, "a tactile sensor using magnetoelastic material has been developed, where the material was bonded to a substrate, and then used as a core for an inductor. As the core is stressed, the material's susceptibility changed, which is measured as a change in the coil's inductance".

B-5 Optical sensors

The operating principles of optical sensors fall into two classes:

- **Intrinsic**. This is where the optical phase, polarization, or intensity of the transmitted light are modulated without interference of the optical path
- **Extrinsic**. This is where the physical stimulus interacts with the light external to the primary optical path.

According to Crowder, the extrinsic sensor based on intensity measurement is the most widely used for robotic touch and force sensing, due to its simplicity of construction and the subsequent information processing.

One method of constructing such a sensor is by placing source-receiver fibre pairs in a solid elastomer structure as shown in Figure B-2.

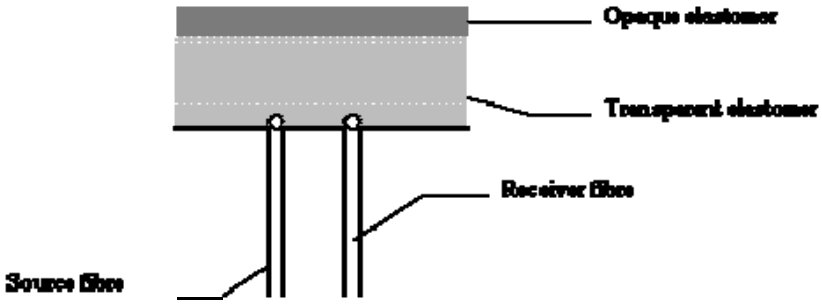

Figure B-2: Optical based sensor, [11]

As shown in Figure B-2, the source and receiver fibers are embedded in a clear elastomer with a reflective silicon rubber layer at the top. An applied force will change the thickness of the clear elastomer resulting in a change in the amount of light reflected to the receiver. For satisfactory operation the clear elastomer must have a lower compliance that the reflective layer.

Another method is using the phenomena of photoelasticity. This is where stress or strain strain causes birefringence in an optically transparent material. As a force is applied to the

material while light passes through it, the photoelastic material effectively rotates the plane of polarization which results in a change in the light intensity. This change is then effectively a function of the applied force.

Both these methods for touch sensing are complex and will require a lot of work to manufacture and define the relationship between light intensity and applied force.

B-6 Piezoelectric sensors

Piezoelectricity is the ability of certain materials to generate an electric charge when subjected to an external mechanical stress. Materials that exhibit this property are usually crystals and some ceramics, but polymers such as polyvinylidene fluoride (PVDF) are normally used in sensors. Polyvinylidene Fluoride is not piezoelectric in its raw state, but it is made piezoelectric by heating it within an electric field.

The attractive thing of polyvinylidene fluoride is that it is supplied in thin sheets of between 5 μm and 2 mm thick and it is coated with a thin layer of metallization to collect the charge and permit the desired electrical connections to be made.

B-7 Strain gauges

A strain gauge detects the change in length of a material it is attached to when the material is subjected to an external force. A typical strain gauge is manufactured from either a resistive element or a semiconductor material.

A semi-conducting strain gauge is fabricated from a suitable doped piece of silicone. In such a case the mechanism used for the resistance change is the piezoresistive effect. The sensors can be manufactures in a matrix within the silicone giving a robust and reliable tactile sensor.

B-8 Force sensing resistor

A force sensing resistor (FSR) is a piezoresistivity conductive polymer. Application of a force to the surface of a FSR will result in a change in resistance in a predictable manner. It is normally supplied as a polymer sheet which has had the sensing film applied by screen printing. The sensing film consists of both electrically conducting and non-conducting particles suspended in matrix. When a force is applied to the surface, this causes the particles to come in contact with the conducting electrodes, resulting in a change in resistance of the film.

As with all resistive based sensors the FSR requires a relatively simple interface as it is only necessary to measure the resistance. FSRs are also manufactured to reduce temperature dependence, improve mechanical properties and increase surface durability. Another advantage is that FSRs can be specifically manufactured into existing arrays of a couple of microns thick.

APPENDIX C: FSR DATASHEET

The following data is quoted verbatim from promotional literature provided by Interlink Electronics. This information is being reproduced without their permission and is subject to revocation.

Interlink
Electronics
Carpinteria, CA 93013
PO Box 40760
Santa Barbara, CA
93140

Tel: 805/684-2100
Fax: 805/684-8282

What's An FSR?

The Force Sensing Resistor™ is a polymer thick film (PTF) device which exhibits a decrease in resistance with any increase in force applied to the active surface. Its force sensitivity is optimized for use in human touch control of electronic devices. The FSR is not a load cell or strain gauge. Though it has similar properties, it is not suited for precision equipment.

Force vs. Resistance

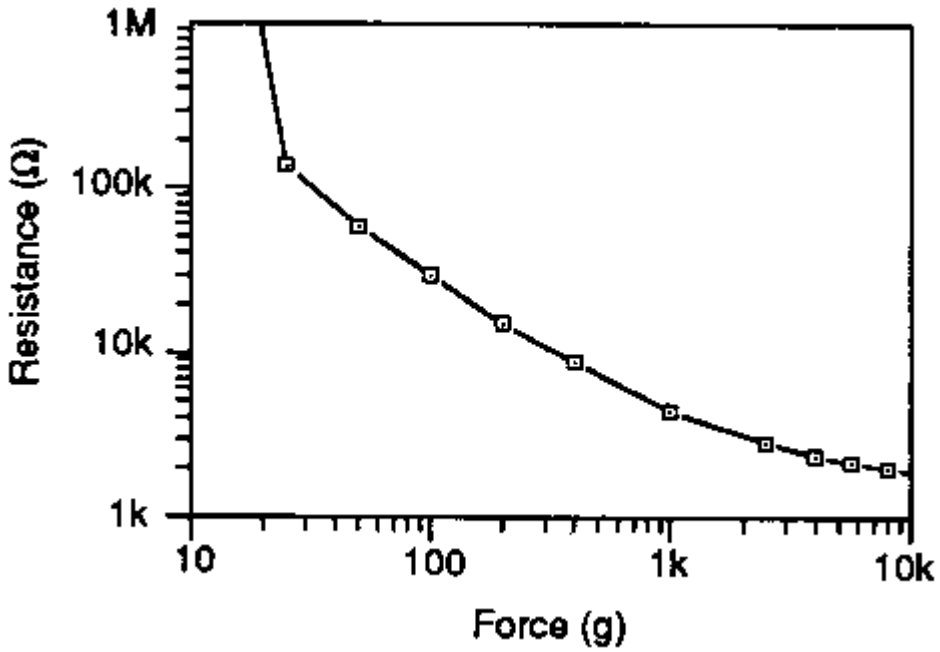

The FSR force vs. resistance characteristic shown in Figure 1

provides an overview of the FSR's typical response behavior. For interpretational convenience, the force vs. resistance data are plotted on a log/log format. These data are representative of our typical devices, with this particular force vs. resistance characteristic being the response of standard part #152 (1.27cm diameter circle) with a 0.6mm thick silicone rubber (50 durometer) overlay and using a 0.56 cm diameter flat probe for actuation. In general, the FSR's response approximately follows a power-law characteristic.

At the low force end of the force-resistance characteristic a switch-like response is evident. This threshold, or "break force", that swings the resistance from greater than 1MΩ to about 50-100 kΩ (the beginning of the power-law) is controlled by the top substrate material and overlay thickness and flexibility. At the high force end of the dynamic range, the response deviates from the power-law behavior, and eventually saturates to a point where increases in force yield little or no decrease in resistance.

Force vs. Conductance

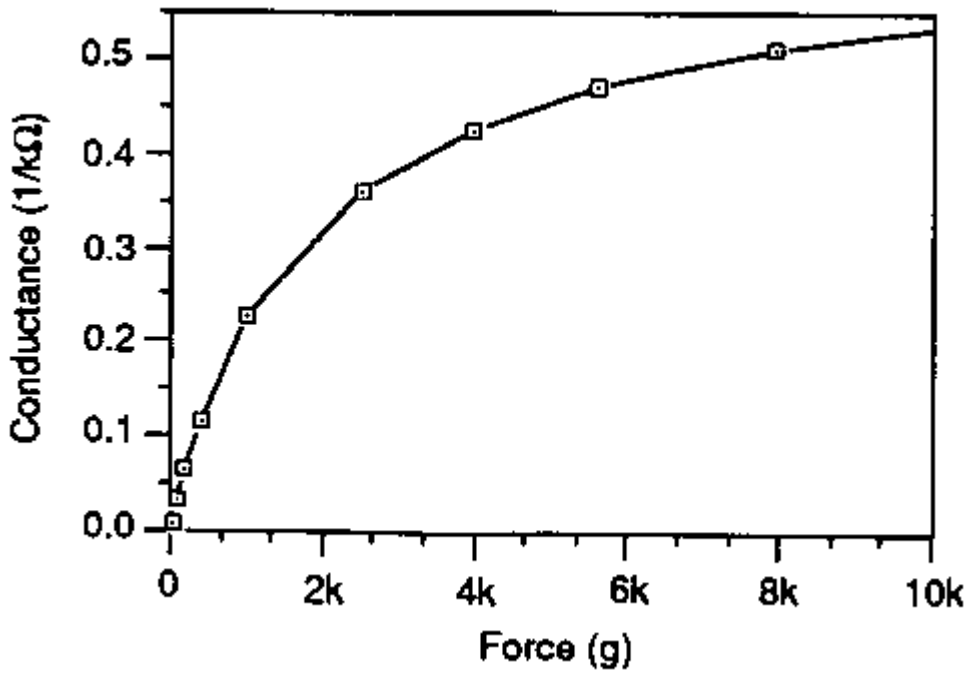

In Figure 2, force vs. conductance (1/resistance) is shown. This format allows simpler interpretation on a linear scale. Notice that the response is in the range of 0-2kg, which is common to human interface applications, is very linear. A simple circuit called a current-to-voltage converter (see TechNote; Suggested Interfaces 1-7) takes advantage of this inverse proportionality and can be useful where response linearity is desired.

FSR™ Technical Specifications

These are typical parameters. FSR's are custom devices and can be made for use outside these specifications. Consult Applications Engineering with your specific requirements.

Simple FSRs and Arrays

Parameter	Value	Conditions
Size Range	Max = 20" x 30" (51 x 76 cm) Min = 0.2" x 0.2" (0.5 x 0.5 cm)	Any shape
Device Thickness	0.008" to 0.050" (0.20 to 1.25 mm)	
Force Sensitivity Range	30g to 10kg	
Pressure Sensitivity Range	0.45psi to 150psi (0.03 kg/cm^2 to 10 kg kg/cm^2)	30g to 10kg 1 cm^2 actuator
Part to Part Force Repeatability	± 15% full scale	For typical part with consistent actuation
Single Part Force Repeatability	± 2% full scale	
Force Resolution	Better than 0.5% full scale	
Break Force	30 to 100g (1 to 3.5 oz) typical	Dependent on probe size/shape
Stand-Off Resistance	> 1MΩ	
Switch Characteristic	Essentially zero travel	
Device Rise Time	1-2msec (mechanical)	
Lifetime	>10 million actuations	
Use Temperature	-30ºC to 170ºC	High temperature adhesives
Maximum Current	1 mA/cm^2 of applied force	
Sensitivity to Noise/Vibration	Not significantly affected	
EMI/ESD	Passive device -- not damaged by EMI or ESD	
Lead Attachment	Standard flex circuit techniques	See TechNote

For Linear Pots and XYZ Pads

Parameter	Value	Conditions

Positional Resolution	0.003" (0.075 mm) typical	1 cm wide actuator
Positional Accuracy	<±1% full scale	

APPENDIX D: KOGE AIR PUMP

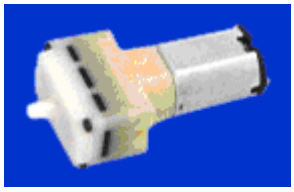

KPM12A

Inquire

Specifications

1. Rated Voltage	DC3.0V
2.Rated Current	<460mA
3.Inflation Time	<8.0 S (From 0 to 300 mmHg in a 100CC tank.)
4. Air Flow Without Load	>1.0LPM
5. Max. Pressure	>350mmHg
6. Leakage	Max. 3 mmHg/min from 300mmHg at 100CC tank.
7. Noise Level	65dB (30cm away)
8. Apply For	Air

PHYSICAL DIMENSION

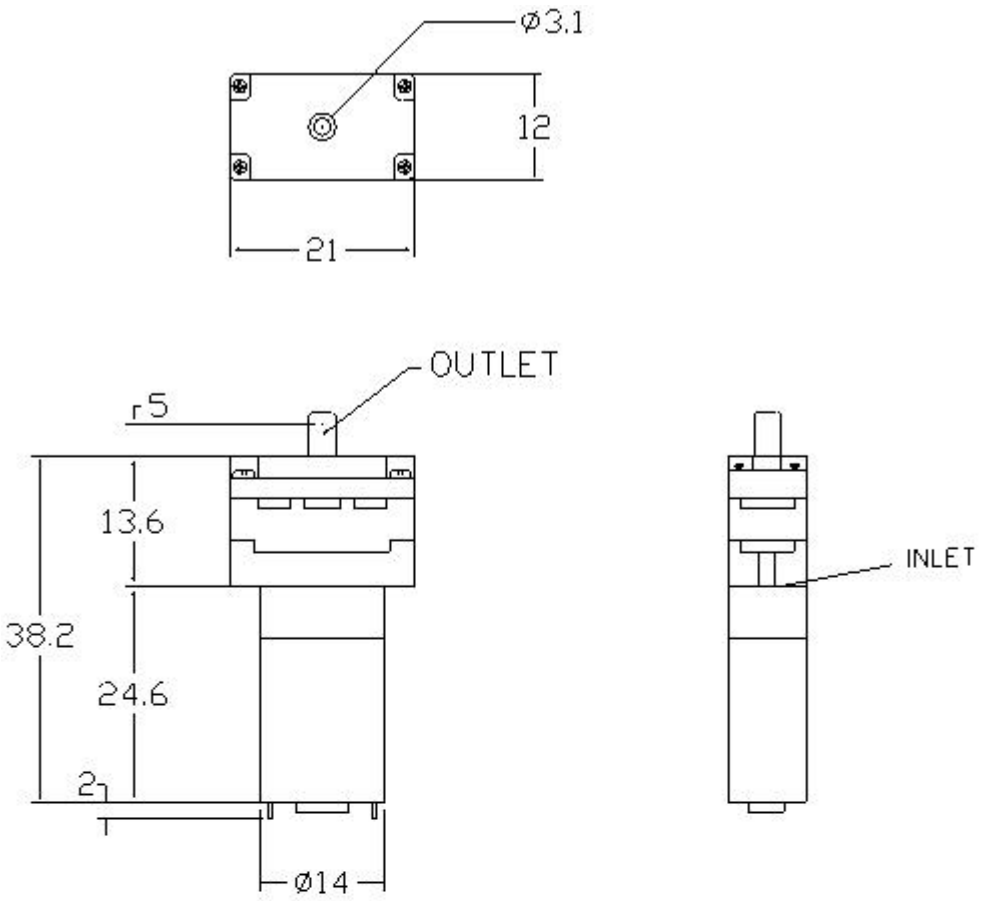

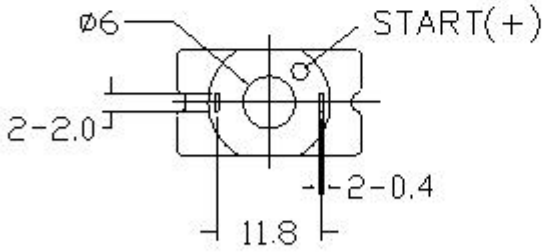

Unit:mm

APPENDIX E: FESTO PRESSURE SENSOR

Pressure sensors SDE1, with display

Product overview

FESTO

- Five pressure measuring ranges
- Measurement of relative or differential pressure
- Switch outputs PNP, NPN and with analogue current or voltage output
- LCD or illuminated LCD display
- Wide range of connection and mounting options

Detailed product information
➔ www.festo.com/catalogue/sde1

Product overview

Method of measurement	Measured variable	Pressure measuring range [bar]	Switching function	Pneumatic connection	Type of mounting	Electrical output	
						Digital	Analogue
Piezoresistive pressure sensor with display	Relative pressure Differential and relative pressure	0 ... –1 –1 ... +1 0 ... 2 0 ... 6 0 ... 10	Freely programmable	Male thread R1/8, R1/4 Female thread G1/8 Push-in fitting for tubing OD 4 mm	On DIN H-rail Via wall/surface bracket On service unit Front panel mounting	PNP	–
						2x PNP	–
						PNP	0 ... 10 V
						PNP	4 ... 20 mA
						2x PNP	4 ... 20 mA
						NPN	–
						2x NPN	–
						NPN	0 ... 10 V
						NPN	4 ... 20 mA

APPENDIX F: DATA ACQUISITION BOX COMMANDS AND SPECIFICATIONS

COMMANDS:

"HELP" – this will display all the commands that can be entered
"VERSION" – this will display the version number of the data acquisition box
"READ ALL" – this command will read all the analog inputs
"READ ADR" – this command will read the analog input at the specified address. ADR must be a value between 0 and 47.

If an invalid command is entered the program will display an error message and it will list all the above information.

Entering a recognized command such as READ ALL or READ ADR will measure the voltage at the specified sensor terminal, convert it to a digital value and display it as ADC*nn* = *value checksum*. Here *nn* refers to the number of the sensor chosen (0-47), *value* is the measured value between 0-1023 and *checksum* is a number used to check if the data was correctly send via the RS232 ort. Checksum is the sum of the individual digits of the measured value. If the measured value is 657 for example, the checksum value should be 18. If this is not the case, then the data was not sent properly.
Table F-1 shows the technical specifications of the data acquisition box.

Table F-1: Specifications of data acquisition box

Supply Voltage	8 – 20 Volt
Supply current	Less than 50 mA
Number of channels	48
Channel resolution	10 bit
Sampling rate	1 Hz or slower
Serial Communication parameters	8 Data bits 1 Stop bit No parity No flow-control 9600 baud rate